Wind and Structures, Vol. 11, No. 2 (2008) 153-178
DOI: http://dx.doi.org/10.12989/was.2008.11.2.153

Wind-induced lateral-torsional coupled responses of tall buildings

J. R. Wu[1,2] and Q. S. Li*[2]

[1]*Department of Civil Engineering, Jinan University, Guangzhou 510632, China*
[2]*Department of Building and Construction, City University of Hong Kong Tat Chee Avenue, Kowloon, Hong Kong*

Alex Y. Tuan

Department of Civil Engineering, Tam Kang University, Taipei, Taiwan
(Received February 21, 2005, Accepted March 3, 2008)

Abstract. Based on the empirical formulas for power spectra of generalized modal forces and local fluctuating wind forces in across-wind and torsional directions, the wind-induced lateral-torsional coupled response analysis of a representative rectangular tall building was conducted by setting various parameters such as eccentricities in centers of mass and/or rigidity and considering different torsional to lateral stiffness ratios. The eccentricity effects on the lateral-torsional coupled responses of the tall building were studied comprehensively by structural dynamic analysis. Extensive computational results indicated that the torsional responses at the geometric center of the building may be significantly affected by the eccentricities in the centers of mass and/or rigidity. Covariance responses were found to be in the same order of magnitude as the along-wind or across-wind responses in many eccentricity cases, suggesting that the lateral-torsional coupled effects on the overall wind-induced responses can not be neglected for such situations. The calculated results also demonstrated that the torsional motion contributed significantly to the total responses of rectangular tall buildings with mass and/or rigidity eccentricities. It was shown through this study that the framework presented in this paper provides a useful tool to evaluate the wind-induced lateral-torsional coupled responses of rectangular buildings, which will enable structural engineers in the preliminary design stages to assess the serviceability of tall buildings, potential structural vibration problems and the need for a detailed wind tunnel test.

Keywords: tall building; wind-induced vibration; wind tunnel test; dynamic analysis.

1. Introduction

Tall buildings under wind action usually oscillate simultaneously in along-wind and across-wind directions as well as in torsional modes. While several procedures have been developed for predicting wind-induced loads and responses in along-wind direction (Davenport 1967), accurate analytical methods for estimating across-wind and torsional response have not been possible yet. However, for tall buildings with aspect ratios over 5, their across-wind responses usually exceed the

* Cheung Kong Chair Professor, Corresponding Author, E-mail: bcqsli@cityu.edu.hk

along-wind responses (Islam, *et al*. 1992, Li 2000). On the other hand, wind-induced torsional vibration of tall buildings can enlarge the displacement and acceleration near the peripheries of their cross section; especially when the side faces of a rectangular tall building are wider, and/or it is asymmetric, and/or its lowest torsional natural frequency is approaching to the lowest translational nature frequency, wind-induced torsional responses may become the main part of the total responses for the peripheral points of the building. Meanwhile, habitants in a tall building are more sensible of torsional motion than translational motion (Tallin 1984). Hence, it is important to accurately evaluate the across-wind and torsional responses for the design and analysis of tall buildings.

It is well known that the mechanisms of across-wind and torsional wind loads on tall buildings are much more complex than those of along-wind dynamic loads. The mechanical transfer function, relating the loads to the response, is simple and straightforward. However, the aerodynamic transfer function, relating the gust structure to the wind-induced forces in across-wind and torsional direction, is difficult to establish without aids from wind tunnel tests. Over the past three decades, wind tunnel test has been proved and recognized as an important tool in civil engineering practices (Cermak 2003). Traditionally, multi-degrees-of freedom aeroelastic models are usually used to study the behaviors of wind-sensitive structures (Isyumov 1982). Although such a technique provides the most direct and reliable estimations, required model making is usually expensive and time consuming. Alternatively, High-Frequency Force Balance (HFFB) technique was developed to measure the overturning moments directly (Tschanz, *et al.* 1983), in case that the aerodynamic damping effects are negligible. Another method, Synchronous Multi-Pressure Scanning System (SMPSS), allows simultaneous measurements of pressure at many points on model surfaces, as well as determination of instantaneous overall wind forces from the local pressure measurements. Based on HFFB and SMPSS model tests, obtained wind loads can be used to calculate structural responses by vibration analysis method.

Although no general analytical methods with sufficient accuracy are available for obtaining across-wind and torsional wind loads (Li 2000, Lin, *et al.* 2005), through extensive wind tunnel tests, some empirical formulas have been proposed for the power spectral densities of fluctuating lift and torque for rectangular tall buildings with different side and aspect ratios. Among these empirical formulas, some were obtained from extensive HFFB model test results (Choi and Kanda 1993, AIJ 1996, Zhou, *et al.* 2003). Others were derived based on pressure measurements on surfaces of building models through SMPSS tests (Liang, *et al.* 2002, Li, *et al.* 2004, Liang 2004). While wind tunnel test is not available, or time is limited in the preliminary design stage, such empirical formulas for the aerodynamics wind forces can serve as useful tools to evaluate the wind-induced responses and serviceability of rectangular tall buildings (Li, *et al.* 2004, Liang, *et al.* 2005). If vibration modes of a structure are uncoupled, the along-wind, across-wind and torsional responses could be evaluated by considering the two orthogonal fundamental sway modes and the first torsional mode independently. This treatment is valid only if the centers of mass and rigidity are coincident with the geometry center of the building and the generalized wind loads in the three directions are uncorrelated (Islam, *et al.* 1992). However, modern tall buildings are often structurally asymmetric because of their irregular building shapes and non-symmetrical lateral resisting forces. Their centers of aerodynamic forces, centers of mass and centers of rigidity are often non-coincident. Therefore, their wind-induced lateral and torsional responses are coupled in such cases. A study of coupled responses of asymmetric tall buildings was conducted by Kan and Chopra (1976) in seismic analysis of structures. The wind-induced responses of asymmetric tall buildings were investigated by a number of researchers (Tallin 1984, Tallin, *et al.* 1985, Safak, *et al.* 1987, Islam, *et al.* 1992, Katagiri, *et al.* 1992, Kareem 1992a, 1992b, Chen and Kareem 2005). However, literature

review reveals that there is a lack of comprehensive and comparative study conducted to investigate the wind-induced lateral-torsional responses of tall buildings based on both HFFB and SMPSS model test results with consideration of effects of various parameters such as eccentricities in centers of mass and/or rigidity and torsional to lateral stiffness ratios. Therefore, there is a need to carry out such a study to comprehensively investigate the wind-induced lateral-torsional responses of tall buildings.

Based on the empirical formulas for the power spectra of the aerodynamics wind forces in across-wind and torsional directions obtained from extensive HFFB and SMPSS model tests, this paper is concerned with a comprehensive investigation on the wind-induced lateral-torsional motions of rectangular tall buildings. The eccentricity effects on the lateral-torsional responses of a rectangular tall building are evaluated by setting various eccentricities in center of mass or/and rigidity and considering different ratio of torsional and lateral stiffness. The computational results show that the framework presented in this paper is effective to estimate the wind-induced lateral-torsional coupled responses of rectangular tall buildings.

2. Lateral-torsional coupled wind-induced response analysis

A 3-dimensional (3D) analytical model of an *N*-story rectangular tall building is shown in Fig. 1. *Z*-axis is chosen as a vertical line that passes the geometric center of the building. For simplification, the following assumptions are made in this study:

(1) For all stories, the principal axis of resistance is identical and oriented along *X*- and *Y*- axis shown in Fig. 1.

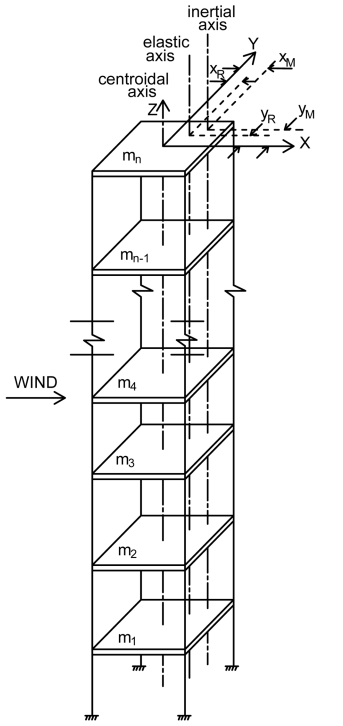

Fig. 1 The full 3D analytical model of the tall building

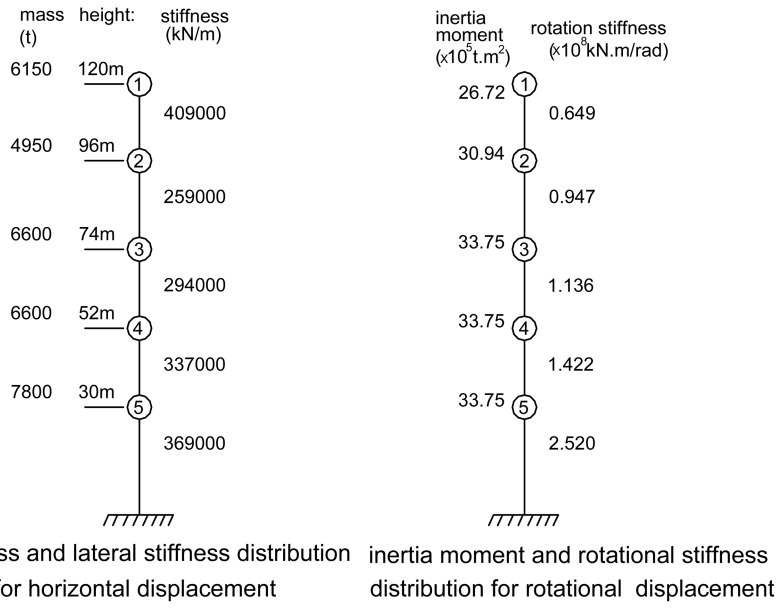

Fig. 2 Vertical distributions of lumped mass, inertia moment and lateral stiffness in translational and rotation directions

(2) The same eccentricities in center of mass and center of rigidity are assumed for all stories.
(3) All stories have the same radius of gyration.

As shown in Fig. 1, coordinates of the center of mass and center of rigidity are (x_M, u_M) and (x_R, y_R), respectively. The lumped mass at each floor has three degrees of freedom: translational displacements in X and Y direction; and rotational displacement in Z direction. The equation of motion of the $3N$ degrees-of-freedom system can be expressed in the following matrix form (Kan and Chopra 1976, Saiful 1988):

$$\begin{bmatrix} \boldsymbol{M}_{xx} & 0 & \boldsymbol{M}_{x\theta} \\ 0 & \boldsymbol{M}_{yy} & \boldsymbol{M}_{y\theta} \\ \boldsymbol{M}_{x\theta}^T & \boldsymbol{M}_{y\theta}^T & \boldsymbol{M}_{\theta\theta} \end{bmatrix} \begin{Bmatrix} \ddot{\boldsymbol{u}} \\ \ddot{\boldsymbol{v}} \\ \ddot{\boldsymbol{\theta}} \end{Bmatrix} + \begin{bmatrix} \boldsymbol{C}_{xx} & 0 & \boldsymbol{C}_{x\theta} \\ 0 & \boldsymbol{C}_{yy} & \boldsymbol{C}_{y\theta} \\ \boldsymbol{C}_{x\theta}^T & \boldsymbol{C}_{y\theta}^T & \boldsymbol{D}_{\theta\theta} \end{bmatrix} \begin{Bmatrix} \dot{\boldsymbol{u}} \\ \dot{\boldsymbol{v}} \\ \dot{\boldsymbol{\theta}} \end{Bmatrix} + \begin{bmatrix} \boldsymbol{K}_{xx} & 0 & \boldsymbol{K}_{x\theta} \\ 0 & \boldsymbol{K}_{yy} & \boldsymbol{K}_{y\theta} \\ \boldsymbol{K}_{x\theta}^T & \boldsymbol{K}_{y\theta}^T & \boldsymbol{K}_{\theta\theta} \end{bmatrix} \begin{Bmatrix} \boldsymbol{u} \\ \boldsymbol{y} \\ \boldsymbol{\theta} \end{Bmatrix} = \begin{Bmatrix} \boldsymbol{F}_x \\ \boldsymbol{F}_y \\ \boldsymbol{F}_\theta \end{Bmatrix} \tag{1}$$

All sub-matrices in Equation (1) are of order $N \times N$ and sub-vectors are $N \times 1$, the mass sub-matrices are

$$\boldsymbol{M}_{xx} = \boldsymbol{M}_{yy} = \boldsymbol{M} = \begin{bmatrix} m_1 & & & \\ & m_2 & & \\ & & .. & \\ & & & m_N \end{bmatrix}, \quad \boldsymbol{M}_{\theta\theta} = \begin{bmatrix} \hat{r}_1^2 m_1 & & & \\ & \hat{r}_2^2 m_2 & & \\ & & .. & \\ & & & \hat{r}_N^2 m_N \end{bmatrix}$$

$$\boldsymbol{M}_{x\theta} = -Y_M \boldsymbol{M}, \quad \boldsymbol{M}_{y\theta} = -X_M \boldsymbol{M}, \quad \hat{r}_j = \sqrt{X_M^2 + Y_M^2 + r_j^2} \quad (j = 1, 2, \ldots N) \tag{2}$$

where r_j is the radius of gyration for m_j, defined at the mass center

The corresponding stiffness sub-matrices in the global stiffness matrix are defined as

$$\boldsymbol{K}_{xx} = \begin{bmatrix} k_{1x} + k_{2x} & -k_{2x} & & & & & \\ -k_{2x} & k_{2x} + k_{3x} & -k_{3x} & & & & \\ & -k_{3x} & k_{3x} + k_{4x} & -k_{4x} & & & \\ & & & .. & .. & .. & \\ & & & -K_{(N-1)x} & k_{(N-1)x} + k_{Nx} & -k_{Nx} & \\ & & & & -k_{Nx} & k_{Nx} & \end{bmatrix}$$

$$\boldsymbol{K}_{yy} = \begin{bmatrix} k_{1y} + k_{2y} & -K_{2y} & & & & & \\ -k_{2y} & k_{2y} + k_{3y} & -k_{3y} & & & & \\ & -k_{3y} & k_{3y} + k_{4y} & -k_{4y} & & & \\ & & & .. & .. & .. & \\ & & & -k_{(N-1)y} & k_{(N-1)y} + k_{Ny} & -k_{Ny} & \\ & & & & -K_{Ny} & K_{Ny} & \end{bmatrix}$$

$$\hat{\boldsymbol{K}}_{\theta\theta} = \begin{bmatrix} \hat{k}_{1\theta}+\hat{k}_{2\theta} & -\hat{k}_{2\theta} & & & & & \\ -\hat{k}_{2\theta} & \hat{k}_{2\theta}+\hat{k}_{3\theta} & -\hat{k}_{3\theta} & & & & \\ & -\hat{k}_{3\theta} & \hat{k}_{3\theta}+\hat{k}_{4\theta} & -\hat{k}_{4\theta} & & & \\ & & & .. & .. & .. & \\ & & & -\hat{k}_{(N-1)\theta} & \hat{k}_{(N-1)\theta}+\hat{k}_{N\theta} & -\hat{k}_{N\theta} & \\ & & & & -\hat{k}_{N\theta} & \hat{k}_{N\theta} & \end{bmatrix}$$

$$\boldsymbol{K}_{x\theta} = -Y_R\,\boldsymbol{K}_{xx}, \quad \boldsymbol{K}_{y\theta} = X_R\boldsymbol{K}_{yy}, \quad \hat{k}_{j\theta} = k_{j\theta}+Y_R^2k_{jx}+X_R^2k_{jy} \quad (j = 1, 2, \ldots N) \tag{3}$$

where k_{jx}, k_{jy} are the lateral stiffness in X and Y direction for the j-th floor, respectively and $k_{j\theta}$ is the torsional stiffness for the j-th floor, in the geometric center of the original uncoupled structure without eccentricity. F_x, F_y and F_θ are wind loads in X-, Y- and Z- axis, respectively.

2.1. Wind-induced response analysis based on the 3D analytical model

Since the vibration modes of the full 3D analytical model described in Eq. (1) are multi-coupled in general, the wind-induced responses in along-wind, across-wind and torsional directions can not be solved independently. Hence, the Complete Quadratic Combination (CQC) method should be used for evaluating the wind-induced lateral-torsional coupled responses for this type of structures.

As mentioned previously, wind-induced dynamic responses of most tall buildings primarily occur in the fundamental along-wind and across-wind modes as well as the first torsional vibration mode (Li, *et al.* 2004). Therefore, the displacement vector involved in Eq. (1) can be expressed, approximately, in terms of the first three coupled vibration modes. i.e.,

$$\boldsymbol{d} = \{\boldsymbol{u}\ \boldsymbol{v}\ \boldsymbol{\theta}\}^T = [\{\boldsymbol{\phi}\}^{(1)}\ \{\boldsymbol{\phi}\}^{(2)}\ \{\boldsymbol{\phi}\}^{(3)}]\{q_1\ q_2\ q_3\}^T = \boldsymbol{\phi q} \tag{4}$$

where $\boldsymbol{\phi}$ is the coupled modal matrix and q_k is the k-th generalized coordinate, which indicates the contribution of the k-th mode $\{\boldsymbol{\phi}\}^{(k)}$ to the displacement vector $\boldsymbol{d}$. Assuming the Rayleigh damping model to be used in this study, the equation of motion of this damped system with $3 \times N$ DOFs can be transformed to the following equation by pre-multiplying both sides of Eq. (1) by $\{\boldsymbol{\phi}\}^{(k)}$.

$$\ddot{q}_k + 2\omega_k\xi_k\dot{q}_k + \omega_k^2q_k = \frac{f_k}{m_k^*}, \qquad k = 1, 2, 3 \tag{5}$$

where $f_k = \{\boldsymbol{\phi}\}^{(k)T}\{\boldsymbol{F}\}$ is the k-th generalized modal force and m_k^* is the k-th generalized modal mass.

For the wind-induced aerodynamic loads, the spectral density of the generalized coordinate can be expressed in terms of the spectral density of the generalized force as:

$$S_{q_kq_l}(\omega) = H_k(i\omega)S_{f_kf_l}(\omega)H_l^*(i\omega), \quad i = \sqrt{-1}, \quad k, l = 1, 2, 3 \tag{6}$$

The frequency response function $H_k(i\omega)$ is defined as

$$H_k(i\omega) = \frac{1}{m_k^*[(\omega_k^2-\omega^2)+2i\xi_k\omega_k\omega]} \tag{7}$$

The RMS value of the generalized coordinate can be expressed as follows:

$$\sigma_{qk}^2 = \int_0^\infty |H_k(i\omega)|^2 S_{f_k}(\omega)\, d\omega = \frac{1}{\omega_k^4 m_k^{*2}} \int_0^\infty \frac{S_{f_k}(\omega)}{\left[\left(1-\left(\frac{\omega}{\omega_k}\right)^2\right)^2 + 4\xi_k^2\left(\frac{\omega}{\omega_k}\right)^2\right]}\, d\omega \qquad k = 1, 2, 3 \tag{8}$$

Through the same procedure, the covariance values of the generalized coordinate can be determined by

$$\sigma_{q_k q_l} = \int_0^\infty Re\{S_{q_k q_l}(\omega)\}\, d\omega = \int_0^\infty [R_{kl}(\omega) S_{f_k f_l}^C(\omega) - I_{kl}(\omega) S_{f_k f_l}^Q(\omega)]\, d\omega \qquad k, l = 1, 2, 3 \tag{9}$$

where S^C and S^Q are the real and imaginary parts of the cross-spectra, respectively. R_{kl} and I_{kl} are the real and imaginary parts of $\{H_k(i\omega)H_l^*(i\omega)\}$, which are defined by:

$$R_{kl}(\omega) = \frac{\left[\left\{1-\left(\frac{\omega}{\omega_k}\right)^2\right\}\left\{1-\left(\frac{\omega}{\omega_l}\right)^2\right\} + 4\xi_k\xi_l\frac{\omega^2}{\omega_k\omega_l}\right]}{\omega_k^2\omega_l^2 m_k^* m_l^*\left[\left(1-\left(\frac{\omega}{\omega_k}\right)^2\right)^2 + 4\xi_k^2\left(\frac{\omega}{\omega_k}\right)^2\right]\left[\left(1-\left(\frac{\omega}{\omega_k}\right)^2\right)^2 + 4\xi_l^2\left(\frac{\omega}{\omega_l}\right)^2\right]}$$

$$I_{kl}(\omega) = \frac{2\omega\left[\frac{\xi_k}{\omega_k}\left\{1-\left(\frac{\omega}{\omega_k}\right)^2\right\} - \frac{\xi_l}{\omega_l}\left\{1-\left(\frac{\omega}{\omega_l}\right)^2\right\}\right]}{\omega_k^2\omega_l^2 m_k^* m_l^*\left[\left(1-\left(\frac{\omega}{\omega_k}\right)^2\right)^2 + 4\xi_k^2\left(\frac{\omega}{\omega_k}\right)^2\right]\left[\left(1-\left(\frac{\omega}{\omega_l}\right)^2\right)^2 + 4\xi_l^2\left(\frac{\omega}{\omega_l}\right)^2\right]} \tag{10}$$

The RMS and covariance values of the responses at the geometric center of each floor can be obtained from the relationship given in Eq. (4). Then, Eq. (8) can be further expressed as:

$$\begin{aligned}
\sigma_{d_j}^2 &= \sum_{k=1}^{3} \phi_j^{(k)2}\sigma_{q_k}^2 + 2\sum_{k=1}^{2}\sum_{l=k+1}^{3} \phi_j^{(k)}\phi_j^{(l)}\sigma_{q_k q_l} \\
\sigma_{d_j d_m} &= \sum_{k=1}^{3} \phi_j^{(k)}\phi_m^{(k)}\sigma_{q_k}^2 + 2\sum_{k=1}^{2}\sum_{l=k+1}^{3} \phi_j^{(k)}\phi_m^{(l)}\sigma_{q_k q_l} \qquad j, m = 1, 2, \ldots 3N
\end{aligned} \tag{11}$$

$$\begin{aligned}
\sigma_{\dot{d}_j}^2 &= \sum_{k=1}^{3} \phi_j^{(k)2}\sigma_{\dot{p}_k}^2 + 2\sum_{k=1}^{2}\sum_{l=k+1}^{3} \phi_j^{(k)}\phi_j^{(l)}\sigma_{\dot{q}_k \dot{q}_l} \\
\sigma_{\dot{d}_j \dot{d}_m} &= \sum_{k=1}^{3} \phi_j^{(k)}\phi_m^{(k)}\sigma_{\dot{q}_k}^2 + 2\sum_{k=1}^{2}\sum_{l=k+1}^{3} \phi_j^{(k)}\phi_m^{(l)}\sigma_{\dot{q}_k \dot{q}_l} \qquad j, m = 1, 2, \ldots 3N
\end{aligned} \tag{12}$$

As the along-wind, across-wind and torsional displacements at the geometric center of the top floor are denoted as u_N, v_N, θ_N, respectively, the wind-induced responses at the upper-right corner (see Fig. 1) of the top floor can be obtained from the responses at the geometric center, which can be expressed as

$$\begin{cases} u_{Nc} = u_N + \dfrac{B}{2}\theta_N & \ddot{u}_{Nc} = \ddot{u}_{Nc} + \dfrac{B}{2}\ddot{\theta}_N \\ v_{Nc} = v_N + \dfrac{D}{2}\theta_N & \ddot{v}_{Nc} = \ddot{v}_{Nc} + \dfrac{D}{2}\ddot{\theta}_N \end{cases} \tag{13}$$

where B and D represent the building width and depth, respectively. The RMS responses at the upper-right corner of the top floor can then be determined by

$$\begin{cases} \sigma_{u_{Nc}} = \sqrt{\sigma_{u_N}^2 + \dfrac{B^2}{4}\sigma_{\theta_N}^2 - B\sigma_{u_N\theta_N}} & \sigma_{v_{Nc}} = \sqrt{\sigma_{v_N}^2 + \dfrac{D^2}{4}\sigma_{\theta_N}^2 + D\sigma_{v_N\theta_N}} \\ \sigma_{\ddot{u}_{Nc}} = \sqrt{\sigma_{\ddot{u}_N}^2 + \dfrac{B^2}{4}\sigma_{\ddot{\theta}_N}^2 - B\sigma_{\ddot{u}_N\ddot{\theta}_N}} & \sigma_{\ddot{v}_{Nc}} = \sqrt{\sigma_{\ddot{v}_N}^2 + \dfrac{D^2}{4}\sigma_{\ddot{\theta}_N}^2 + D\sigma_{\ddot{v}_N\ddot{\theta}_N}} \end{cases} \tag{14}$$

2.2. Response analysis based on HFFB model tests

The analysis procedure given in section 2.1 was based on that the power spectra densities of the local fluctuating along-wind, across-wind and torsional wind forces could be obtained from SMPSS wind tunnel tests or empirical formulas. However, in many cases, HFFB model test technique is used in wind-resistant design of tall buildings because of its higher efficiency and lower cost. From HFFB model tests, the aerodynamic overturning base moments acting on a tall building can be obtained. By utilizing the overturning base moments from HFFB tests to evaluate the wind-induced lateral-torsional response, a reduced 3DOFs model which includes two translational DOFs and one torsional DOF is used instead of a full 3D model.

As reported by Kan and Chopra (1977), any lower vibration modes of a torsionally coupled building may be approximated as linear combination of three vibration modes of the corresponding torsionally uncoupled system by assuming that center of geometric, center of mass and center of rigidity are coincident while all other properties are identical to the actual lateral-torsional coupled system. The mode shapes of this kind of structural system would be approximately determined from the eigenvalue solutions of the following equation.

$$\begin{bmatrix} \boldsymbol{M}_{xx} & 0 & 0 \\ 0 & \boldsymbol{M}_{yy} & 0 \\ 0 & 0 & \boldsymbol{M}_{\theta\theta} \end{bmatrix} \begin{Bmatrix} \ddot{\boldsymbol{u}} \\ \ddot{\boldsymbol{v}} \\ \ddot{\boldsymbol{\theta}} \end{Bmatrix} + \begin{bmatrix} \boldsymbol{K}_{xx} & 0 & 0 \\ 0 & \boldsymbol{K}_{yy} & 0 \\ 0 & 0 & \boldsymbol{K}_{\theta\theta} \end{bmatrix} \begin{Bmatrix} \boldsymbol{u} \\ \boldsymbol{v} \\ \boldsymbol{\theta} \end{Bmatrix} = \begin{Bmatrix} 0 \\ 0 \\ 0 \end{Bmatrix} \tag{15}$$

The solutions of Eq. (15) give the eigenvectors that define the vibration mode shape matrix $\boldsymbol{\phi}$ with the form: $\boldsymbol{\phi} = \begin{bmatrix} \boldsymbol{\phi}_{xx} & & \\ & \boldsymbol{\phi}_{yy} & \\ & & \boldsymbol{\phi}_{\theta\theta} \end{bmatrix}$. Normally the first vibration mode shape in each direction is sufficient for evaluating the wind-induced response of a tall building. The mode shapes will satisfy the following orthogonal conditions:

$$\begin{cases} \{\phi_{xx}\}^{(1)^T} M_{xx} \{\phi_{xx}\}^{(1)} = m_{xx}^{*(1)} & \{\phi_{xx}\}^{(1)^T} \boldsymbol{K}_{xx} \{\phi_{xx}\}^{(1)} = k_{xx}^{*(1)} \\ \{\phi_{yy}\}^{(1)^T} M_{yy} \{\phi_{yy}\}^{(1)} = m_{yy}^{*(1)} & \{\phi_{yy}\}^{(1)^T} \boldsymbol{K}_{yy} \{\phi_{yy}\}^{(1)} = k_{yy}^{*(1)} \\ \{\phi_{\theta\theta}\}^{(1)^T} M_{TT} \{\phi_{\theta\theta}\}^{(1)} = m_{\theta\theta}^{*(1)} & \{\phi_{TT}\}^{(1)^T} \boldsymbol{K}_{TT} \{\phi_{\theta\theta}\}^{(1)} = k_{\theta\theta}^{*(1)} \end{cases} \tag{16}$$

Subsequently the displacement in Eq. (1) can be expressed by the following formula using the mode decomposition method:

$$\boldsymbol{d} = \{\boldsymbol{u}\ \boldsymbol{v}\ \boldsymbol{\theta}\}^T = \boldsymbol{\phi}\boldsymbol{q} \tag{17}$$

$$\text{where } \boldsymbol{\phi} = \begin{bmatrix} \{\phi_{xx}\}^{(1)} & & \\ & \{\phi_{yy}\}^{(1)} & \\ & & \{\phi_{\theta\theta}\}^{(1)} \end{bmatrix}, \quad q = \begin{Bmatrix} q_x \\ q_y \\ q_\theta \end{Bmatrix}$$

Substituting Eq. (17) into Eq. (1), pre-multiplying both sides by $\boldsymbol{\phi}^T$ and making use of the orthogonal conditions yields the following Eq.:

$$\begin{bmatrix} m_{xx}^{*(1)} & 0 & m_{x\theta}^{*(1)} \\ 0 & m_{yy}^{*(1)} & m_{y\theta}^{*(1)} \\ m_{xT}^{*(1)} & m_{y\theta}^{*(1)} & m_{\theta\theta}^{*(1)} \end{bmatrix} \begin{Bmatrix} \ddot{q}_x \\ \ddot{q}_y \\ \ddot{q}_\theta \end{Bmatrix} + \begin{bmatrix} c_{xx}^{*(1)} & 0 & c_{x\theta}^{*(1)} \\ 0 & c_{yy}^{*(1)} & c_{y\theta}^{*(1)} \\ c_{x\theta}^{*(1)} & c_{y\theta}^{*(1)} & c_{\theta\theta}^{*(1)} \end{bmatrix} \begin{Bmatrix} \dot{q}_x \\ \dot{q}_y \\ \dot{q}_\theta \end{Bmatrix} + \begin{bmatrix} k_{xx}^{*(1)} & 0 & k_{x\theta}^{*(1)} \\ 0 & k_{yy}^{*(1)} & k_{y\theta}^{*(1)} \\ k_{x\theta}^{*(1)} & k_{y\theta}^{*(1)} & k_{\theta\theta}^{*(1)} \end{bmatrix} \begin{Bmatrix} q_x \\ q_y \\ q_\theta \end{Bmatrix} = \begin{Bmatrix} f_x^* \\ f_y^* \\ f_\theta^* \end{Bmatrix} \tag{18}$$

where f_x^*, f_y^*, f_θ^* are actually the generalized modal forces of the fundamental mode in the *X, Y* and *Z* direction, respectively.

When the mode shape of the fundamental sway vibration mode is a straight line varying linearly with building height and that of the first torsional mode has a constant magnitude, the generalized modal forces f_x^*, f_y^*, f_θ^* are proportional to the overturning base moments, which can then be measured from HFFB model tests directly. In case that nonlinear mode shapes are presented, the measured results should be adjusted to correct for the differences in the mode shapes, and the actual generalized modal forces can then be obtained (Vickery, *et al.* 1985, Holmes 1987, Xu and Kwok 1987, Holmes, *et al.* 2003, Chen and Kareem 2005). The modification factor for the power spectral densities of the generalized modal forces in each direction can be calculated by

$$\begin{aligned} \eta_x &= \sqrt{\frac{S_{f_x^*}(n)}{S_{My}(n)}} = \sqrt{\frac{\int_0^H \int_0^H \sigma_{F_x}(z,n)\sigma_{F_x}(z',n)R_{F_x}(z,z',n)\phi_{xx}^{(1)}(z)\phi_{xx}^{(1)}(z')dzdz'}{\int_0^H \int_0^H \sigma_{F_x}(z,n)\sigma_{F_x}(z',n)R_{F_x}(z,z',n)\phi_{M_y}(z)\phi_{M_y}(z')dzdz'}} \\ \eta_y &= \sqrt{\frac{S_{f_y^*}(n)}{S_{Mx}(n)}} = \sqrt{\frac{\int_0^H \int_0^H \sigma_{F_y}(z,n)\sigma_{F_y}(z',n)R_{F_y}(z,z',n)\phi_{yy}^{(1)}(z)\phi_{yy}^{(1)}(z')dzdz'}{\int_0^H \int_0^H \sigma_{F_y}(z,n)\sigma_{F_y}(z',n)R_{F_y}(z,z',n)\phi_{M_x}(z)\phi_{M_x}(z')dzdz'}} \\ \eta_\theta &= \sqrt{\frac{S_{f_\theta^*}(n)}{S_{M_\theta}(n)}} = \sqrt{\frac{\int_0^H \int_0^H \sigma_{F_\theta}(z,n)\sigma_{F_\theta}(z',n)R_{F_\theta}(z,z',n)\phi_{\theta\theta}^{(1)}(z)\phi_{\theta\theta}^{(1)}(z')dzdz'}{\int_0^H \int_0^H \sigma_{F_\theta}(z,n)\sigma_{F_\theta}(z',n)R_{F_\theta}(z,z',n)\phi_{M_\theta}(z)\phi_{M_\theta}(z')dzdz'}} \end{aligned} \tag{19}$$

where $\sigma_{F_i}(z, n)R_{F_i}(z, z', n)\big|_{(i = x, y, \theta)}$ are the RMS values of the wind forces at height z and the coherence functions of local fluctuating wind forces, respectively. $\phi_{M_i}(z)\big|_{(i = x, y, \theta)}$ is the mode shape of the building used in HFFB model tests, which take the form of z/H in X and Y direction and remain the value of 1 in Z direction, respectively.

Eq. (18) represents the reduced 3DOFs model of the concerned building. Its features are almost the same as those of the full 3D analytical model described by Eq. (1), with a major difference in degrees of freedom. For the full 3D analytical model, there are $3N$ DOFs, while only 3 DOFs are considered in the reduced 3DOFs model. Once the power spectral densities of the generalized modal forces $S_{f_x^*}$, $S_{f_y^*}$, $S_{f_\theta^*}$ are determined, the wind-induced lateral-torsional coupled responses can be determined by the procedure similar to that described by Eqs. (2)~(14).

3. Empirical formulas for fluctuating wind loads

3.1. The power spectra of local fluctuating wind force

Before the wind-induced lateral-torsional coupled responses of a tall building are calculated£¨the power spectra of the aerodynamic wind forces on the building should be obtained from wind tunnel tests or other methods.

Assuming a tall building has N lumped masses shown in Fig. 1, and each lumped mass has two translational DOFs in X and Y direction and one rotational DOF in Z direction. Then the spectral density of the fluctuating along-wind force on each lumped mass can be expressed by

$$S_{F_x}(z_i, z_j, f) = (\rho C_D)^2 A_{z_i} A_{z_j} V_{z_i} V_{z_j} \sqrt{S_V(z_i, f) S_V(z_j, f)}\, Coh(z_i, z_j, f) \tag{20}$$

where A_{z_i}, V_{z_i} are tributary area and mean wind speed for the lumped mass located at height Z_i, $Coh(z_i, z_j, f)$ is coherence function of fluctuating wind speeds at different height. $S_V(z_i, f)$ is the auto-power spectral density of the along-wind (longitudinal) fluctuating wind speed, which can be represented by the widely-used von Karman spectrum (Simiu and Scanlan 1996):

$$\frac{f S_V(z_i, f)}{\sigma_{V z_i}^2} = \frac{4\dfrac{f L_V}{V_{z_i}}}{\left(1 + 70.8\left(\dfrac{f \times L_V}{V_{z_i}}\right)^2\right)^{5/6}} \tag{21}$$

As no accurate analytical methods to predict across-wind forces and torsional moments are currently available, it is desirable to estimate such wind effects with aids from wind tunnel tests. Some empirical formulas for power spectral densities of local fluctuating lift and torque on rectangular tall buildings with different side and aspect ratios have been proposed based on extensive SMPSS wind tunnel tests (Liang, *et al.* 2002, 2005, Liang 2004). After comparison of the performance of the existing empirical formulas based on the available wind tunnel test results and field measurements (Li, *et al.* 2004), it was decided that the empirical formula for the spectrum of fluctuating across-wind force proposed by Liang, *et al*. (2002) and that of fluctuating torsional moment established by Liang (2004) were adopted in this study.

According to Liang, *et al*. (2002), the co-spectral density for the fluctuating across-wind forces along building height is expressed as follows:

$$S_{F_y}(z_i, z_j, f) = \left(\frac{1}{2}\rho C_L\right)^2 A_{z_i} A_{z_j} V_{z_i}^2 V_{z_j}^2 \sqrt{S_{F_y}^*(z_i, f) S_{F_y}^*(z_j, f)}\, Coh(z_i, z_j, f) \tag{22}$$

where $S_{F_y}^*(z_i, f) = \dfrac{S_{F_y}(z_i, f)}{\left(\frac{1}{2}\rho V_{z_i}^2 C_L B\right)^2}$

The normalized power spectral density of the fluctuating across-wind force at height z_i, ($\dfrac{fS_{F_y}(z_i, f)}{\sigma_{F_y}^2}$), can be represented by the following equations (Liang, *et al*. 2002):

$$\frac{fS_{F_y}^*(z_i, f)}{\sigma_{F_y}^2} = A \cdot \frac{H(C_1)\overline{f}^2}{(1-\overline{f}^2)^2 + C_1\overline{f}^2} + (1-A) \cdot \frac{C_2^{0.5}\overline{f}^3}{1.56[(1-\overline{f}^2)^2 + 2\overline{f}^2]} \quad \text{for } \frac{1}{4} \le D/B < 3 \tag{23}$$

$$\frac{fS_{F_y}(z_i, f)}{\sigma_{F_y}^2} = A \cdot \frac{1.275\overline{f}^2}{(1-\overline{f}^2)^2 + C_1\overline{f}^2} + (1-A)\frac{C_2^{0.5}\left(\dfrac{\overline{f}}{\overline{k}}\right)^3}{1.56\left[\left(1-\dfrac{\overline{f}^2}{\overline{k}^2}\right)^2 + \dfrac{C_2\overline{f}^2}{\overline{k}^2}\right]} \quad \text{for } 3 \le D/B \le 4 \tag{24}$$

Other parameters involved in Eqs. (22)~(24) can be found in Liang, *et al*. (2002).

The normalized power spectral density of the fluctuating torsional moment along building height z_i, ($\dfrac{fS_{F_\theta}(z_i, f)}{\sigma_{F_\theta}^2}$), is expressed as follows (Liang 2004):

$$\begin{cases} \dfrac{fS_{F_\theta}(f)}{\sigma_{F_\theta}^2} = B_0 F(f) + \dfrac{fS_{ST}(f)}{\sigma_{ST}^2} + B_1\dfrac{fS_{VS}(f)}{\sigma_{VS}^2} + B_2\dfrac{fS_{FP}(f)}{\sigma_{FP}^2} \\ \dfrac{fS_{ST}(f)}{\sigma_{ST}^2} = \dfrac{\overline{f}_s/\overline{k}}{[1+\overline{\xi}(\overline{f}_s/\overline{k})^{c_1}]^{c_2}}, \qquad \dfrac{fS_{VS}(f)}{\sigma_{VS}^2} = \dfrac{1}{\delta_1\sqrt{2\pi}} e^{-0.5\left(\frac{\ln \overline{f}_s + 0.5\delta_1^2}{\delta_1}\right)^2} \\ \dfrac{fS_{FP}(f)}{\sigma_{FP}^2} = \dfrac{1}{\delta_2\sqrt{2\pi}} e^{-0.5\left(\frac{\ln \overline{f}_m + 0.5\delta_2^2}{\delta_2}\right)^2} \end{cases} \tag{25}$$

All the other parameters appeared in Eq. (25) are given in Liang (2004).

3.2. The power spectra of overturning moments or generalized modal forces from HFFB wind tunnel tests

Empirical formulas for power spectra of overturning moments in across-wind and torsional direction were proposed by Choi and Kanda (1993) among others based on HFFB wind tunnel tests. It was testified through comparison with available wind tunnel test results and field measurements

that these formulas could provide more accurate results than other existing formulas for predicting across-wind and torsional responses of isolated rectangular tall buildings with various geometrical situations. Therefore, the formulas proposed by Choi and Kanda (1993) were adopted in this study to generate the input forces for the dynamic analysis of the reduced 3DOFs model. The normalized power spectral density of the overturning moment in across-wind direction, $\frac{fS_{M_y}(f)}{\sigma_{M_y}^2}$, is expressed as (Choi and Kanda 1993):

$$\begin{cases} \dfrac{fS_{M_y}(f)}{\sigma_{M_y}^2} = B_1\dfrac{fS_{ST}(f)}{\sigma_{ST}^2} + (1-B_1)\dfrac{fS_{VS}(f)}{\sigma_{VS}^2} \\ \dfrac{fS_{ST}(f)}{\sigma_{ST}^2} = 1.26\dfrac{\bar{f}/\bar{k}}{(1+(\bar{f}/\bar{k})^{1.26})^{5/1.26}} \\ \dfrac{fS_{VS}(f)}{\sigma_{VS}^2} = \dfrac{1}{\delta\sqrt{2\pi}}e^{-0.5\left(\frac{\ln\bar{f}+0.5\delta^2}{\delta}\right)^2} \\ \bar{f} = f/f_s \quad f_s = 0.12\dfrac{V_H/B}{(1+0.38(D/B)^2)^{0.89}} \end{cases} \tag{26}$$

The normalized power spectral density of the overturning moment in torsional direction, $\frac{fS_{M_\theta}(f)}{\sigma_{M_\theta}^2}$, is (Choi and Kanda 1993):

$$\begin{cases} \dfrac{fS_{M_\theta}(f)}{\sigma_{M_\theta}^2} = B_2F_1(\psi_1)\left\{\dfrac{fS_{ST}(f)}{\sigma_{ST}^2} + B_3F_2(\psi_2)\dfrac{fS_{VS}(f)}{\sigma_{VS}^2} + B_4\dfrac{fS_{FP}(f)}{\sigma_{FP}^2}\right\} \\ \dfrac{fS_{FP}(f)}{\sigma_{FP}^2} = \dfrac{1}{\delta_m\sqrt{2\pi}}e^{-0.5\left(\frac{\ln\bar{f}_m+0.5\delta_m^2}{\delta_m}\right)^2}, \qquad \bar{f}_m = f/f_m,\ f_m = 0.15\dfrac{V_H}{\sqrt{BD}} \\ F_1(\psi_1) = \{1+1.5\sin(\psi_1)\}^{-1}, \qquad \psi_1 = \pi/\{1+(\bar{f}_s/1.5)^3\} \\ F_2(\psi_2) = e^{-\bar{f}_s/\gamma}\cos(\psi_2), \qquad \psi_2 = \pi/\{1-\{1+(\bar{f}_s/\gamma)^{1.5}\}^{-1}\} \end{cases} \tag{27}$$

The expressions of $\frac{fS_{ST}(f)}{\sigma_{ST}^2}$, $\frac{fS_{ST}(f)}{\sigma_{VT}^2}$ in Eq. (30) are the same as those in Eq. (29). All other parameters in Eqs. (29) and (30) can be found in Choi and Kanda (1993).

4. The lateral-torsional responses of torsionally coupled rectangular tall buildings

To illustrate the effect of eccentricities in centers of mass and/or rigidity on the wind-induced lateral-torsional response of tall buildings, a typical rectangular building was considered in this study. The rectangular tall building is a 30-storey steel structure with a cross-section area of 40 m × 40 m and 120 m in height, and the average mass density is approximate 187.5 kg/m^3. It was assumed that the isolated tall building was located in a typical suburban terrain, which corresponds

to that the exponent α in the mean wind speed profile is 1/7 for such a terrain (Li 2000). Wind tunnel test was carried out for this building to determine wind forces on the building using pressure measurement technique, and the along-wind, across-wind and torsional responses of the building were calculated based on the model test results (Yoshida, *et al.* 1992). The analytical model of the building for the dynamic analysis was simplified as a cantilever shear column with five lumped masses; each lumped mass has two translational DOFs in horizontal directions (X and Y direction) and one rotational DOF in vertical (Z) direction, as shown in Fig. 2. In other words, the building was modeled as a structural system with 15 DOFs. The lateral stiffness in the two orthogonal translational directions was assumed to be identical. The vertical distributions of the lumped mass, inertia moment, equivalent lateral stiffness of this building in the translational and rotation directions are shown in Fig. 2 (Yoshida, *et al.* 1992). The fundamental natural frequency of this building is 0.336Hz in the two translational directions and 0.313Hz in the torsional direction. Damping ratio was assumed to be 1% for all the vibration modes (Li, *et al*. 1998, 2005).

To examine the reliability and effectiveness of the computational procedure presented in Eqs. (20) to (27), the along-wind, across-wind and torsional responses of the tall building without eccentricity were calculated and compared with the available wind tunnel test results (Yoshida, *et al.* 1992), as shown in Tables 1a and 1b, for the case that the mean wind speeds atop the building were 20 m/s and 30 m/s and the approaching wind was normal to one side of the square building. The satisfactory agreement between the calculated results and the experimental data demonstrates the

Table 1a Wind-induced responses of the tall building (V_H=20 m/s)

RMS Responses		Methods	Lumped mass no.				
			5	4	3	2	1
Along-wind responses	$\sigma_{\dot{U}_j}$ (gal)	Wind tunnel results	0.191	0.332	0.467	0.573	0.620
		Numerical results	0.197	0.374	0.53	0.602	0.673
		Difference	3%	11%	12%	5%	8%
	σ_{U_j} (cm)	Wind tunnel results	0.062	0.119	0.169	0.206	0.219
		Numerical results	0.06	0.118	0.173	0.217	0.278
		Difference	-3%	-1%	2%	5%	21%
Across-wind responses	$\sigma_{\dot{V}_j}$ (gal)	Wind tunnel results	0.554	0.860	1.109	1.329	1.447
		Numerical results	0.526	0.800	1.023	1.134	1.243
		Difference	-5%	-8%	-8%	-17%	-16%
	σ_{V_j} (cm)	Wind tunnel results	0.081	0.15	0.205	0.241	0.252
		Numerical results	0.075	0.123	0.178	0.221	0.265
		Difference	-8%	-22%	-15%	-9%	5%
Torsional responses	$\frac{B}{2}\sigma_{\dot{\theta}_j}$ (gal)	Wind tunnel results	0.067	0.105	0.151	0.195	0.234
		Numerical results	0.057	0.09	0.155	0.209	0.266
		Difference	-18%	-17%	3%	7%	12%
	$\frac{B}{2}\sigma_{\theta_j}$ (cm)	Wind tunnel results	0.012	0.026	0.042	0.053	0.062
		Numerical results	0.013	0.035	0.059	0.079	0.096
		Difference	8%	26%	29%	33%	35%

Table 1b Wind-induced responses of the tall building (V_H=30 m/s)

RMS Responses		Methods	Lumped mass no.				
			5	4	3	2	1
Along-wind responses	$\sigma_{\ddot{U}_j}$ (gal)	Wind tunnel results	0.583	1.024	1.434	1.771	1.913
		Numerical results	0.580	1.090	1.530	1.910	2.060
		Difference	-1%	6%	6%	7%	7%
	σ_{U_j} (cm)	Wind tunnel results	0.158	0.307	0.442	0.542	0.577
		Numerical results	0.180	0.370	0.540	0.670	0.710
		Difference	12%	17%	18%	19%	19%
Across-wind responses	$\sigma_{\ddot{V}_j}$ (gal)	Wind tunnel results	0.608	1.035	1.44	1.767	1.907
		Numerical results	0.710	1.400	2.070	2.580	2.770
		Difference	14%	26%	30%	32%	31%
	σ_{V_j} (cm)	Wind tunnel results	0.207	0.391	0.544	0.649	0.685
		Numerical results	0.268	0.500	0.740	0.920	0.990
		Difference	23%	22%	26%	29%	31%
Torsional responses	$\frac{B}{2}\sigma_{\ddot{\theta}_j}$ (gal)	Wind tunnel results	0.223	0.57	0.637	0.823	0.983
		Numerical results	0.183	0.452	0.505	0.679	0.822
		Difference	-22%	-26%	-26%	-21%	-20%
	$\frac{B}{2}\sigma_{\theta_j}$ (cm)	Wind tunnel results	0.04	0.095	0.15	0.198	0.232
		Numerical results	0.036	0.098	0.165	0.221	0.263
		Difference	-11%	3%	9%	10%	12%

good applicability of the framework presented above.

Based on the empirical formulas for the power spectra of the aerodynamic wind loads, the wind-induced lateral-torsional responses of the tall building were evaluated when different eccentricities in centers of mass and/or rigidity were assumed. The mean wind speed atop the building was assumed to be V_H = 20 m/s in the dynamic analysis. The wind-induced along-wind, across-wind and torsional responses at the geometry center and the building corners were calculated. By comparing the results with those from the cases without the eccentricity, the effects of the eccentricities on the wind-induced responses of the tall building can be assessed.

4.1. Lateral-torsional coupled response (considering eccentricity in center of mass)

First of all, the along-wind, across-wind and torsional RMS displacement and acceleration responses at the geometry center and upper-right corner atop the building are presented, with consideration of eccentricities in the mass center in along-wind direction (referred to as the along-wind eccentricities in this paper) while the eccentricities in rigidity center and eccentricity in mass center in the across-wind direction were set to equal to zero. Assuming V_H is 20 m/s. Table 2 lists the calculated wind-induced responses for nine eccentricity cases (cases 1 ~ 9), in which case 0 represents the case without any eccentricity in the building. The rotational response is expressed as linear response at a distance of half width (B/2) from the geometry center, both in Table 2 and

Table 2 Wind-induced lateral-torsional coupled responses atop the building with the along-wind eccentricities in the mass center only

	Case No.	Coordinate of mass and rigidity center (m)	RMS response at geometric center			RMS response at corner ($B/2$, $D/2$)		Covariance response between U_N, V_N **and** θ_N		
		(x_M, y_M, x_R, y_R)	σ_{U_N}	σ_{V_N}	$\frac{B}{2}\sigma_{\theta_N}$	$\sigma_{U_{N_c}}$	$\sigma_{V_{N_c}}$	$\sigma_{U_N V_N}$	$\sqrt{B}\sigma_{U_N\theta_N}$	$\sqrt{B}\sigma_{V_N\theta_N}$
displacement (cm)	case 0	(0,0,0,0)	0.2778	0.3903	0.0963	0.2940	0.4020	0.0000	0.0000	0.0000
	case 1	(1,0,0,0)	0.2778	0.3780	0.1410	0.3115	0.3010	0.0000	0.0000	-0.2687
	case 2	(2,0,0,0)	0.2778	0.3624	0.1812	0.3316	0.2661	0.0000	0.0000	-0.3055
	case 3	(3,0,0,0)	0.2778	0.3536	0.1993	0.3419	0.2644	0.0000	0.0000	-0.3080
	case 4	(4,0,0,0)	0.2778	0.3490	0.2078	0.3469	0.2693	0.0000	0.0000	-0.3041
	case 5	(5,0,0,0)	0.2778	0.3463	0.2122	0.3496	0.2745	0.0000	0.0000	-0.2993
	case 6	(6,0,0,0)	0.2778	0.3445	0.2148	0.3511	0.2790	0.0000	0.0000	-0.2949
	case 7	(-1,0,0,0)	0.2778	0.3780	0.1410	0.3115	0.4847	0.0000	0.0000	0.2687
	case 8	(-2,0,0,0)	0.2778	0.3624	0.1812	0.3316	0.5074	0.0000	0.0000	0.3055
	case 9	(-3,0,0,0)	0.2778	0.3536	0.1993	0.3419	0.5096	0.0000	0.0000	0.3080
		(x_M, y_M, x_R, y_R)	$\sigma_{\ddot{U}_N}$	$\sigma_{\ddot{V}_N}$	$\frac{B}{2}\sigma_{\ddot{\theta}_N}$	$\sigma_{\ddot{U}_{N_c}}$	$\sigma_{\ddot{V}_{N_c}}$	$\sigma_{\ddot{U}_N\ddot{V}_N}$	$\sqrt{B}\sigma_{\ddot{U}_N\ddot{\theta}_N}$	$\sqrt{B}\sigma_{\ddot{V}_N\ddot{\theta}_N}$
acceleration (gal)	case 0	(0,0,0,0)	0.6725	1.2427	0.2663	0.7233	1.2709	0.0000	0.0000	0.0000
	case 1	(1,0,0,0)	0.6725	1.1773	0.5050	0.8410	0.9578	0.0000	0.0000	-0.8507
	case 2	(2,0,0,0)	0.6725	1.0955	0.6949	0.9671	0.8750	0.0000	0.0000	-0.9578
	case 3	(3,0,0,0)	0.6725	1.0563	0.7805	1.0303	0.8733	0.0000	0.0000	-0.9810
	case 4	(4,0,0,0)	0.6725	1.0453	0.8242	1.0637	0.8724	0.0000	0.0000	-1.0053
	case 5	(5,0,0,0)	0.6725	1.0500	0.8513	1.0849	0.8632	0.0000	0.0000	-1.0402
	case 6	(6,0,0,0)	0.6725	1.0645	0.8716	1.1009	0.8480	0.0000	0.0000	-1.0834
	case 7	(-1,0,0,0)	0.6725	1.1773	0.5050	0.8410	1.5378	0.0000	0.0000	0.8507
	case 8	(-2,0,0,0)	0.6725	1.0955	0.6949	0.9671	1.6126	0.0000	0.0000	0.9578
	case 9	(-3,0,0,0)	0.6725	1.0563	0.7805	1.0303	1.6393	0.0000	0.0000	0.9810

subsequent tables. Comparing with the wind-induced torsional displacements, the torsional accelerations were found to be more sensitive to variation of the eccentricity in the mass center, as shown in this table. With increase of the eccentricity in the mass center, the across-wind response in the geometry center always decreased while the rotational response in the geometry center tended to increase regardless of the situations of the along-wind eccentricity in the mass center. The positive along-wind eccentricity in the mass center resulted in reduction of the across-wind response at the upper-right corner atop the building as comparing with the case of the negative along-wind eccentricity which magnified the across-wind response at this point significantly. Although the across-wind response decreased due to the positive along-wind eccentricity, an increase in the torsional response may be critical as far as the serviceability of the tall building is concerned. Comparing the results of Case 1 with those of other cases shown in the table, the across-wind response was no longer a dominant component as it did for a mechanically uncoupled building. Actually, in some cases, the covariance response between the across-wind and torsional directions

Table 3 Wind-induced lateral-torsional coupled responses atop the building with the across-wind eccentricities in the mass center only

	Case No.	Coordinate of mass and rigidity center (m)	RMS response at geometric center			RMS response at corner ($B/2$, $D/2$)		Covariance response between U_N, V_N **and** θ_N		
		(x_M, y_M, x_R, y_R)	σ_{U_N}	σ_{V_N}	$\frac{B}{2}\sigma_{\theta_N}$	$\sigma_{U_{N_c}}$	$\sigma_{V_{N_c}}$	$\sigma_{U_N V_N}$	$\sqrt{B}\sigma_{U_N\theta_N}$	$\sqrt{B}\sigma_{V_N\theta_N}$
displacement (cm)	case 0	(0,0,0,0)	0.2778	0.3903	0.0963	0.2940	0.4020	0.0000	0.0000	0.0000
	case 10	(0,1,0,0)	0.2740	0.3903	0.1078	0.2253	0.4049	0.0038	0.1896	-0.0031
	case 11	(0,2,0,0)	0.2692	0.3903	0.1204	0.1927	0.4085	0.0092	0.2233	0.0010
	case 12	(0,3,0,0)	0.2666	0.3903	0.1268	0.1830	0.4104	0.0127	0.2316	0.0003
	case 13	(0,4,0,0)	0.2651	0.3903	0.1300	0.1811	0.4114	0.0147	0.2332	0.0002
	case 14	(0,5,0,0)	0.2642	0.3903	0.1318	0.1817	0.4120	0.0159	0.2328	0.0002
	case 15	(0,6,0,0)	0.2636	0.3903	0.1330	0.1831	0.4124	0.0165	0.2316	0.0007
	case 16	(0,-1,0,0)	0.2740	0.3903	0.1078	0.3502	0.4049	0.0038	-0.1896	0.0031
	case 17	(0,-2,0,0)	0.2692	0.3903	0.1204	0.3699	0.4085	0.0092	-0.2233	-0.0010
	case 18	(0,-3,0,0)	0.2666	0.3903	0.1268	0.3752	0.4104	0.0127	-0.2316	-0.0003
		(x_M, y_M, x_R, y_R)	$\sigma_{\ddot{U}_N}$	$\sigma_{\ddot{V}_N}$	$\frac{B}{2}\sigma_{\ddot{\theta}_N}$	$\sigma_{\ddot{U}_{N_c}}$	$\sigma_{\ddot{V}_{N_c}}$	$\sigma_{\ddot{U}_N\ddot{V}_N}$	$\sqrt{B}\sigma_{\ddot{U}_N\ddot{\theta}_N}$	$\sqrt{B}\sigma_{\ddot{V}_N\ddot{\theta}_N}$
acceleration (gal)	case 0	(0,0,0,0)	0.6725	1.2427	0.2663	0.7233	1.2709	0.0000	0.0000	0.0000
	case 10	(0,1,0,0)	0.6411	1.2427	0.3447	0.5823	1.2895	0.0016	0.4367	-0.0120
	case 11	(0,2,0,0)	0.6020	1.2427	0.4218	0.5448	1.3123	0.0021	0.4936	0.0030
	case 12	(0,3,0,0)	0.5833	1.2427	0.4587	0.5412	1.3246	0.0019	0.5078	-0.0014
	case 13	(0,4,0,0)	0.5779	1.2427	0.4776	0.5378	1.3313	0.0014	0.5223	-0.0004
	case 14	(0,5,0,0)	0.5798	1.2427	0.4891	0.5308	1.3355	0.0010	0.5418	0.0008
	case 15	(0,6,0,0)	0.5861	1.2427	0.4974	0.5212	1.3385	0.0007	0.5650	0.0031
	case 16	(0,-1,0,0)	0.6411	1.2427	0.3447	0.8488	1.2896	0.0016	-0.4367	0.0120
	case 17	(0,-2,0,0)	0.6020	1.2427	0.4218	0.8854	1.3123	0.0021	-0.4936	-0.0030
	case 18	(0,-3,0,0)	0.5833	1.2427	0.4587	0.8992	1.3246	0.0019	-0.5078	0.0014

was about in the same order of magnitude as that of the across-wind response at the geometric center, which indicated that the torsional motion contributed significantly to the overall wind-induced responses.

With various across-wind eccentricities in the center of mass (the eccentricity in the rigidity center and the along-wind eccentricity in the mass center were assumed to be zero), the corresponding wind-induced responses (Cases 10 ~ 18) are presented in Table 3. Comparing the results with those in Table 2, it was found that the torsional displacement and acceleration responses seemed less sensitive to the variation of the across-wind eccentricity in the mass center. Meanwhile, the across-wind responses at the upper–right corner atop the building increased regardless of the situation of the across-wind eccentricity in the mass center. It was also shown that the positive across-wind eccentricity in the mass center reduced the along-wind response at the upper-right corner atop the building, as comparing with the case of the negative across-wind eccentricity which clearly magnified the along-wind response. Generally speaking, this is very similar to that observed in Cases 1 ~ 9 for the along-wind response. If the incident wind direction is unknown, one would not

Table 4 Wind-induced lateral-torsional coupled responses atop the building with the eccentricities in the mass center only

Case No.	Coordinate of mass and rigidity center (m)	RMS response at geometric center			RMS response at corner ($B/2$, $D/2$)		Covariance response between U_N, V_N **and** θ_N		
	(x_M, y_M, x_R, y_R)	σ_{U_N}	σ_{V_N}	$\frac{B}{2}\sigma_{\theta_N}$	$\sigma_{U_{N_c}}$	$\sigma_{V_{N_c}}$	$\sigma_{U_N V_N}$	$\sqrt{B}\sigma_{U_N\theta_N}$	$\sqrt{B}\sigma_{V_N\theta_N}$
case 0	(0,0,0,0)	0.2778	0.3903	0.0963	0.2940	0.4020	0.0000	0.0000	0.0000
case 19	(1,1,0,0)	0.2966	0.3639	0.1396	0.2986	0.2808	0.0330	0.1353	-0.2703
case 20	(2,2,0,0)	0.2950	0.3554	0.1654	0.2834	0.2878	0.0111	0.1846	-0.2662
case 21	(3,3,0,0)	0.2954	0.3510	0.1743	0.2839	0.2955	0.0072	0.1925	-0.2575
case 22	(4,4,0,0)	0.2946	0.3497	0.1781	0.2861	0.3008	0.0060	0.1915	-0.2520
case 23	(5,5,0,0)	0.3259	0.3193	0.1800	0.3207	0.2700	0.0254	0.1890	-0.2480
case 24	(6,6,0,0)	0.3257	0.3183	0.1812	0.3228	0.2726	0.0256	0.1863	-0.2446
case 25	(-1,-1,0,0)	0.2966	0.3639	0.1396	0.3546	0.4743	0.0330	-0.1353	0.2703
case 26	(-2,-2,0,0)	0.2950	0.3554	0.1654	0.3853	0.4739	0.0111	-0.1846	0.2662
case 27	(-3,-3,0,0)	0.2954	0.3510	0.1743	0.3933	0.4690	0.0072	-0.1925	0.2575
	(x_M, y_M, x_R, y_R)	$\sigma_{\dot{U}_N}$	$\sigma_{\dot{V}_N}$	$\frac{B}{2}\sigma_{\dot{\theta}_N}$	$\sigma_{\dot{U}_{N_c}}$	$\sigma_{\dot{V}_{N_c}}$	$\sigma_{\dot{U}_N\dot{V}_N}$	$\sqrt{B}\sigma_{\dot{U}_N\dot{\theta}_N}$	$\sqrt{B}\sigma_{\dot{V}_N\dot{\theta}_N}$
case 0	(0,0,0,0)	0.6725	1.2427	0.2663	0.7233	1.2709	0.0000	0.0000	0.0000
case 19	(1,1,0,0)	0.7490	1.1310	0.5045	0.9092	0.8759	0.4391	-0.1062	-0.8755
case 20	(2,2,0,0)	0.8737	0.9842	0.6321	0.9458	0.8831	0.2267	0.5180	-0.7670
case 21	(3,3,0,0)	0.9041	0.9456	0.6794	0.9404	0.9103	0.1749	0.6281	-0.7259
case 22	(4,4,0,0)	0.9193	0.9401	0.7047	0.9291	0.9128	0.1490	0.6917	-0.7396
case 23	(5,5,0,0)	0.9348	0.9452	0.7236	0.9154	0.9036	0.1249	0.7479	-0.7749
case 24	(6,6,0,0)	0.9508	0.9575	0.7409	0.8990	0.8912	0.0945	0.8029	-0.8194
case 25	(-1,-1,0,0)	0.7490	1.1310	0.5045	0.8967	1.5166	0.4391	0.1062	0.8755
case 26	(-2,-2,0,0)	0.8737	0.9842	0.6321	1.1963	1.3988	0.2267	-0.5180	0.7670
case 27	(-3,-3,0,0)	0.9041	0.9456	0.6794	1.2936	1.3721	0.1749	-0.6281	0.7259

know whether the eccentricity in the mass center is in the along-wind or across-wind direction. However, there is usually a dominate wind direction at a specific building site; therefore, the results presented here will still be useful for wind-resistant design of tall buildings.

The lateral-torsional responses of this building are listed in Table 4, with consideration of the existence of both the along-wind and across-wind eccentricities in the mass center (the eccentricity in the rigidity center was set to equal to zero). The results listed in this table show that the eccentricities made the along-wind response at the geometric center increased and the across-wind response at the geometric center decreased. While the eccentricity in the mass center was located at the opposite direction to the upper-right corner of the building, the along-wind and across-wind responses at the upper-right corner atop the building generally increased with increase of the eccentricity in the mass center. The across-wind response at this point decreased in a more sensitive way and its along-wind response remained almost constant when the eccentricity in the mass center was assumed in the same direction as the upper-right corner of the building. Also as shown in this table, in most cases the covariance responses (such as σ_{uw}, σ_{vw}) are almost in the same order of

magnitude as the across-wind response or the along-wind response at the geometric center. In fact, in some cases at the geometric center, the covariance responses (for example, $\sigma_{\ddot{u}\ddot{w}}$, $\sigma_{\ddot{v}\ddot{w}}$) are even as large as the along-wind or across-wind acceleration responses. This implies that the lateral-torsional coupled effect on the overall wind-induced response can not be neglected for such cases.

4.2. Lateral-torsional coupled response (considering eccentricity in center of rigidity)

Parametric studies were also conducted for the cases that only the eccentricities in the rigidity center were presented. If only the along-wind eccentricities in the rigidity center were considered, the lateral-torsional coupled responses are listed in Table 5 for Cases 28~33. The overall trend of variation in the wind-induced response due to the along-wind eccentricities in the rigidity center was almost the same as that shown in Table 2 for the case that only the along-wind eccentricities in the mass center existed. Comparing the results with those in Table 2 for Cases 1~9, it is clear that the positive along-wind eccentricity in the rigidity center magnified the across-wind response at the upper-right corner atop the building while the negative along-wind eccentricity reduced the across-wind response significantly.

While only the across-wind eccentricities in the rigidity center were presented, the corresponding lateral-torsional coupled responses are shown in Table 6 for Cases 34~39. The variation in the wind-induced response due to the across-wind eccentricities in the rigidity center is almost the same as that observed from Table 3 (only the across-wind eccentricities in the mass center existed).

Table 5 Wind-induced lateral-torsional coupled responses atop building with the along-wind eccentricities in the rigidity center only

	Case No.	Coordinate of mass and rigidity center (m)	RMS response at geometric center			RMS response at corner ($B/2$, $D/2$)		Covariance response between U_N, V_N **and** θ_N		
		(x_M, y_M, x_R, y_R)	σ_{U_N}	σ_{V_N}	$\frac{B}{2}\sigma_{\theta_N}$	$\sigma_{U_{N_c}}$	$\sigma_{V_{N_c}}$	$\sigma_{U_N V_N}$	$\sqrt{B}\,\sigma_{U_N\theta_N}$	$\sqrt{B}\,\sigma_{V_N\theta_N}$
displacement (cm)	case 0	(0,0,0,0)	0.2778	0.3903	0.0963	0.2940	0.4020	0.0000	0.0000	0.0000
	case 28	(0,0,1,0)	0.2778	0.3747	0.1491	0.3152	0.4787	0.0000	0.0000	0.2580
	case 29	(0,0,2,0)	0.2778	0.3571	0.1974	0.3408	0.4862	0.0000	0.0000	0.2644
	case 30	(0,0,3,0)	0.2778	0.3525	0.2229	0.3561	0.4717	0.0000	0.0000	0.2205
	case 31	(0,0,-1,0)	0.2778	0.3747	0.1491	0.3152	0.3099	0.0000	0.0000	-0.2580
	case 32	(0,0,-2,0)	0.2778	0.3571	0.1974	0.3408	0.3108	0.0000	0.0000	-0.2644
	case 33	(0,0,-3,0)	0.2778	0.3525	0.2229	0.3561	0.3540	0.0000	0.0000	-0.2205
		(x_M, y_M, x_R, y_R)	$\sigma_{\ddot{U}_N}$	$\sigma_{\ddot{V}_N}$	$\frac{B}{2}\sigma_{\ddot{\theta}_N}$	$\sigma_{\ddot{U}_{N_c}}$	$\sigma_{\ddot{V}_{N_c}}$	$\sigma_{\ddot{U}_N\ddot{V}_N}$	$\sqrt{B}\,\sigma_{\ddot{U}_N\ddot{\theta}_N}$	$\sqrt{B}\,\sigma_{\ddot{V}_N\ddot{\theta}_N}$
acceleration (gal)	case 0	(0,0,0,0)	0.6725	1.2427	0.2663	0.7233	1.2709	0.0000	0.0000	0.0000
	case 28	(0,0,1,0)	0.6725	1.1496	0.5338	0.8586	1.5045	0.0000	0.0000	0.8104
	case 29	(0,0,2,0)	0.6725	1.0259	0.7394	0.9994	1.4959	0.0000	0.0000	0.7992
	case 30	(0,0,3,0)	0.6725	0.9567	0.8278	1.0665	1.4247	0.0000	0.0000	0.6553
	case 31	(0,0,-1,0)	0.6725	1.1496	0.5338	0.8586	0.9746	0.0000	0.0000	-0.8104
	case 32	(0,0,-2,0)	0.6725	1.0259	0.7394	0.9994	0.9800	0.0000	0.0000	-0.7992
	case 33	(0,0,-3,0)	0.6725	0.9567	0.8278	1.0665	1.0821	0.0000	0.0000	-0.6553

Table 6 Wind-induced lateral-torsional coupled responses atop the building with the across-wind eccentricities in the rigidity center only

	Case No.	Coordinate of mass and rigidity center (m)	RMS response at geometric center			RMS response at corner ($B/2$, $D/2$)		Covariance response between U_N, V_N **and** θ_N		
		(x_M, y_M, x_R, y_R)	σ_{U_N}	σ_{V_N}	$\frac{B}{2}\sigma_{\theta_N}$	$\sigma_{U_{N_c}}$	$\sigma_{V_{N_c}}$	$\sigma_{U_N V_N}$	$\sqrt{B}\sigma_{U_N\theta_N}$	$\sqrt{B}\sigma_{V_N\theta_N}$
displacement (cm)	case 0	(0,0,0,0)	0.2778	0.3903	0.0963	0.2940	0.4020	0.0000	0.0000	0.0000
	case 34	(0,0,0,1)	0.2734	0.3903	0.1110	0.3469	0.4058	0.0054	-0.1824	-0.0013
	case 35	(0,0,0,2)	0.2695	0.3903	0.1284	0.3590	0.4109	0.0139	-0.1994	0.0003
	case 36	(0,0,0,3)	0.2705	0.3903	0.1399	0.3557	0.4146	0.0208	-0.1839	-0.0011
	case 37	(0,0,0,-1)	0.2734	0.3903	0.1110	0.2319	0.4058	0.0054	0.1824	0.0013
	case 38	(0,0,0,-2)	0.2695	0.3903	0.1284	0.2222	0.4109	0.0139	0.1994	-0.0003
	case 39	(0,0,0,-3)	0.2705	0.3903	0.1399	0.2428	0.4146	0.0208	0.1839	0.0011
		(x_M, y_M, x_R, y_R)	$\sigma_{\ddot{U}_N}$	$\sigma_{\ddot{V}_N}$	$\frac{B}{2}\sigma_{\ddot{\theta}_N}$	$\sigma_{\ddot{U}_{N_c}}$	$\sigma_{\ddot{V}_{N_c}}$	$\sigma_{\ddot{U}_N\ddot{V}_N}$	$\sqrt{B}\sigma_{\ddot{U}_N\ddot{\theta}_N}$	$\sqrt{B}\sigma_{\ddot{V}_N\ddot{\theta}_N}$
acceleration (gal)	case 0	(0,0,0,0)	0.6725	1.2427	0.2663	0.7233	1.2709	0.0000	0.0000	0.0000
	case 34	(0,0,0,1)	0.6272	1.2427	0.3574	0.8294	1.2930	0.0018	-0.4084	-0.0045
	case 35	(0,0,0,2)	0.5679	1.2427	0.4441	0.8214	1.3196	0.0032	-0.3937	0.0010
	case 36	(0,0,0,3)	0.5358	1.2427	0.4838	0.7835	1.3335	0.0031	-0.3044	-0.0062
	case 37	(0,0,0,-1)	0.6272	1.2427	0.3574	0.5953	1.2930	0.0018	0.4084	0.0045
	case 38	(0,0,0,-2)	0.5679	1.2427	0.4441	0.6040	1.3196	0.0032	0.3937	-0.0010
	case 39	(0,0,0,-3)	0.5358	1.2427	0.4838	0.6546	1.3336	0.0031	0.3044	0.0062

Comparing the results in Table 6 with those in Table 3 for cases 10~18, it was found that the positive across-wind eccentricities in the rigidity center magnified the along-wind response at the upper-right corner, but the negative across-wind eccentricities generally reduced the along-wind response.

The lateral-torsional coupled responses due to both the along-wind and across-wind eccentricities in the rigidity center are shown in Table 7 for Cases 40~45. The results also demonstrated that the along-wind response at the geometric center generally increased and across-wind response at the geometry center normally decreased regardless of the situations of the eccentricities in the rigidity center. Comparing the results with those shown in Table 4, it was found from Table 7 that the across-wind response at the upper-right corner atop the building varied more significant than the along-wind response at this point, in the cases that the eccentricities in the rigidity center were located at the opposite direction to the upper-right corner of the building.

4.3. Lateral-torsional coupled responses (considering eccentricities in centers of mass and rigidity)

As discussed by Islam (1988) and Islam, *et al*. (1992), the eccentricity either in mass center or rigidity center could result in mechanically lateral-torsional coupling motion. Hence, the overall wind-induced response would normally increase due to the eccentricity effect. The wind-induced responses of the building are presented in Table 8 for cases 46~49 that the eccentricities both in the mass center and in the rigidity center coincide at the same location. Comparing these results with

Table 7 Wind-induced lateral-torsional coupled responses atop the building with eccentricities in the rigidity center only

	Case No.	Coordinate of mass and rigidity center (m)	RMS response at geometric center			RMS response at corner ($B/2$, $D/2$)		Covariance response between U_N, V_N **and** θ_N		
		(x_M, y_M, x_R, y_R)	σ_{U_N}	σ_{V_N}	$\frac{B}{2}\sigma_{\theta_N}$	$\sigma_{U_{N_c}}$	$\sigma_{V_{N_c}}$	$\sigma_{U_N V_N}$	$\sqrt{B}\sigma_{U_N\theta_N}$	$\sqrt{B}\sigma_{V_N\theta_N}$
displacement (cm)	case 0	(0,0,0,0)	0.2778	0.3903	0.0963	0.2940	0.4020	0.0000	0.0000	0.0000
	case 40	(0,0,1,1)	0.2995	0.3588	0.1485	0.3531	0.4659	0.0341	-0.1136	0.2574
	case 41	(0,0,2,2)	0.2892	0.3601	0.1833	0.3626	0.4598	0.0042	-0.1193	0.2193
	case 42	(0,0,3,3)	0.2905	0.3648	0.2024	0.3543	0.4465	-0.0068	-0.0106	0.1590
	case 43	(0,0,-1,-1)	0.2995	0.3588	0.1485	0.3144	0.2908	0.0341	0.1136	-0.2574
	case 44	(0,0,-2,-2)	0.2892	0.3601	0.1833	0.3210	0.3394	0.0042	0.1193	-0.2193
	case 45	(0,0,-3,-3)	0.2905	0.3648	0.2024	0.3539	0.3858	-0.0068	0.0106	-0.1590
		(x_M, y_M, x_R, y_R)	$\sigma_{\ddot{U}_N}$	$\sigma_{\ddot{V}_N}$	$\frac{B}{2}\sigma_{\ddot{\theta}_N}$	$\sigma_{\ddot{U}_{N_c}}$	$\sigma_{\ddot{V}_{N_c}}$	$\sigma_{\ddot{U}_N\ddot{V}_N}$	$\sqrt{B}\sigma_{\ddot{U}_N\ddot{\theta}_N}$	$\sqrt{B}\sigma_{\ddot{V}_N\ddot{\theta}_N}$
acceleration (gal)	case 0	(0,0,0,0)	0.6725	1.2427	0.2663	0.7233	1.2709	0.0000	0.0000	0.0000
	case 40	(0,0,1,1)	0.7398	1.1079	0.5336	0.8736	1.4837	0.4537	0.2625	0.8302
	case 41	(0,0,2,2)	0.8453	0.9462	0.6698	1.1033	1.3014	0.2703	-0.2324	0.5913
	case 42	(0,0,3,3)	0.8639	0.9000	0.7143	1.1257	1.2025	0.2410	-0.1036	0.3546
	case 43	(0,0,-1,-1)	0.7398	1.1079	0.5336	0.9492	0.9072	0.4537	-0.2625	-0.8302
	case 44	(0,0,-2,-2)	0.8453	0.9462	0.6698	1.0532	0.9971	0.2703	0.2324	-0.5913
	case 45	(0,0,-3,-3)	0.8639	0.9000	0.7143	1.1162	1.0929	0.2410	0.1036	-0.3546

Table 8 Wind-induced lateral-torsional coupled responses atop the building with eccentricities both in the mass and rigidity center

	Case No.	Coordinate of mass and rigidity center (m)	RMS response at geometric center			RMS response at corner ($B/2$, $D/2$)		Covariance response between U_N, V_N **and** θ_N		
		(x_M, y_M, x_R, y_R)	σ_{U_N}	σ_{V_N}	$\frac{B}{2}\sigma_{\theta_N}$	$\sigma_{U_{N_c}}$	$\sigma_{V_{N_c}}$	$\sigma_{U_N V_N}$	$\sqrt{B}\sigma_{U_N\theta_N}$	$\sqrt{B}\sigma_{V_N\theta_N}$
displacement (cm)	case 0	(0,0,0,0)	0.2778	0.3903	0.0963	0.2940	0.4020	0.0000	0.0000	0.0000
	case 46	(1,1,,1,1)	0.2784	0.3904	0.0996	0.2939	0.4017	-0.0001	0.0315	-0.0315
	case 47	(2,2,2,2)	0.2775	0.3926	0.1087	0.2941	0.4045	-0.0018	0.0486	-0.0486
	case 48	(-1,-1,-1,-1)	0.2784	0.3904	0.0996	0.2973	0.4042	-0.0001	-0.0315	0.0315
	case 49	(-2,-2,-2,-2)	0.2775	0.3926	0.1087	0.3020	0.4103	-0.0018	-0.0486	0.0486
		(x_M, y_M, x_R, y_R)	$\sigma_{\ddot{U}_N}$	$\sigma_{\ddot{V}_N}$	$\frac{B}{2}\sigma_{\ddot{\theta}_N}$	$\sigma_{\ddot{U}_{N_c}}$	$\sigma_{\ddot{V}_{N_c}}$	$\sigma_{\ddot{U}_N\ddot{V}_N}$	$\sqrt{B}\sigma_{\ddot{U}_N\ddot{\theta}_N}$	$\sqrt{B}\sigma_{\ddot{V}_N\ddot{\theta}_N}$
acceleration (gal)	case 0	(0,0,0,0)	0.6725	1.2427	0.2663	0.7233	1.2709	0.0000	0.0000	0.0000
	case 46	(1,1,1,1)	0.6727	1.2428	0.2745	0.7214	1.2698	-0.0004	0.0868	-0.0867
	case 47	(2,2,2,2)	0.6726	1.2438	0.2975	0.7234	1.2720	-0.0028	0.1331	-0.1331
	case 48	(-1,-1,-1,-1)	0.6727	1.2428	0.2745	0.7317	1.2757	-0.0004	-0.0868	0.0867
	case 49	(-2,-2,-2,-2)	0.6726	1.2438	0.2975	0.7474	1.2858	-0.0028	-0.1331	0.1331

those in Tables 2 ~ 7, it is evident that when both the mass center and the rigidity center are located at the same position, the variations of the RMS responses are much less than those of the general

cases that the two centers do not coincide. This is due to the fact that the building behaves almost mechanically uncoupled as the mass center and the rigidity center coincide. Under this situation, only small statistically couplings between the along-wind, across-wind and torsional forces are presented. Therefore, it is easily understood that there is little difference between the results for the cases 46~49 and those for the case without the eccentricities, as shown in Table 8.

4.4. Effect of torsional to lateral stiffness ratio on the lateral-torsional coupled response

As introduced previously, the fundamental torsional natural frequency (0.313 Hz) of the building without eccentricity is close to the first lateral natural frequency (0.336 Hz) in both translational directions. For most symmetric tall buildings where the lateral-force resistant members are located mainly at the periphery of the structure, the fundamental torsional frequency is usually relatively higher than that of the first translational mode. According to Kareem (1992) and Liang, *et al*. (1997), the closeness in magnitudes of the along-wind, across-wind and torsional frequencies may result in amplification of response or redistribution of energy due to the "beat" phenomenon. Therefore, it is necessary to examine the effect of torsional stiffness to lateral stiffness ratio on the wind–induced lateral-torsional coupled responses. For the tall building considered in this study, the calculated results of the lateral-torsional coupled response are shown in Tables 9a and 9b where the torsional stiffness values were respectively assumed to be 1.5, 2 and 2.5 times of the original ones shown in Fig. 2. With increase of the torsional stiffness, the ratios of the first torsional natural frequency to that of the fundamental translational mode are within the range of 1.5 to 2.5. It is shown in Tables 9a and 9b that the RMS torsional response and covariance responses at the geometry center generally decreased with increase of the torsional stiffness. Comparing the results with those in Tables 1 to 7, the RMS torsional response and covariance responses at the geometry center dramatically reduced as the ratio of the torsional to lateral stiffness increased. These results are useful for wind-resistant design of tall buildings. If most of the lateral force resisting members are arranged at the periphery of the building, the overall torsional stiffness of the structure would be enhanced and thus reduce the overall wind-induced responses.

4.5. Response analysis in frequency domain with the reduced 3DOFs model

The response analysis presented in the previous sections was conducted based on the 3D torsionally coupled analytical model and the adopted empirical formulas for the power spectra determined from locally measured wind pressures on surfaces of tall building models. This method allows direct computation of the wind-induced responses and the modal forces of any vibration modes. Although this technique has the advantage of properly determining the generalized forces for nonlinear and/or three dimensional mode shapes, it is required to conduct wind tunnel tests to measure local wind-induced pressures, which is time-consuming and relatively more expensive than the High Frequency Force Balance (HFFB) approach. One the other hand, the HFFB technique can make corrections for nonlinear modes and handle the three-dimensional mode shapes reasonably well. In fact, more databases of overturning moment in across-wind and torsional directions, which were established on the basis of extensive HFFB wind tunnel tests, are available (AIJ 1996, Choi and Kanda 1992, 1993, Zhou, *et al*. 2003). This provides a good opportunity to investigate the lateral-torsional coupled motions of tall buildings from another channel.

In this section, based on the reduced 3DOFs model of the tall building and the empirical formulas

Table 9a Wind-induced lateral-torsional coupled displacement atop the building with different ratios of torsional to lateral stiffness

	Case No.	Coordinate of mass and rigidity center (m)	RMS response at geometric center			RMS response at corner ($B/2$, $D/2$)		Covariance response between U_N, V_N **and** θ_N		
		(x_M, y_M, x_R, y_R)	σ_{U_N}	σ_{V_N}	$\frac{B}{2}\sigma_{\theta_N}$	$\sigma_{U_{N_c}}$	$\sigma_{V_{N_c}}$	$\sigma_{U_N V_N}$	$\sqrt{B}\sigma_{U_N\theta_N}$	$\sqrt{B}\sigma_{V_N\theta_N}$
ratio=1.5	case 0	(0,0,0,0)	0.2778	0.3903	0.0364	0.2801	0.3920	0.0000	0.0000	0.0000
	case 20	(2,2,0,0)	0.2804	0.3851	0.0506	0.2738	0.3881	0.0367	-0.0787	0.0159
	case 41	(0,0,2,2)	0.2903	0.3837	0.0497	0.2805	0.3729	0.0306	-0.0898	0.1030
	case 47	(2,2,2,2)	0.2787	0.3912	0.0417	0.2625	0.3752	-0.0534	0.1025	-0.1185
ratio=2.0	case 0	(0,0,0,0)	0.2778	0.3903	0.0188	0.2784	0.3908	0.0000	0.0000	0.0000
	case 21	(2,2,0,0)	0.2791	0.3885	0.0230	0.2760	0.3891	0.0371	-0.0471	0.0052
	case 41	(0,0,2,2)	0.2493	0.4107	0.0238	0.2385	0.4046	-0.0539	-0.0746	0.0763
	case 47	(2,2,2,2)	0.2783	0.3908	0.0217	0.2685	0.3814	-2.8772	0.0762	-0.0881
ratio=2.5	case 0	(0,0,0,0)	0.2778	0.3903	0.0115	0.2780	0.3905	0.0000	0.0000	0.0000
	case 21	(2,2,0,0)	0.2831	0.3859	0.0135	0.2816	0.3860	0.0348	-0.0320	0.0092
	case 41	(0,0,2,2)	0.2868	0.3848	0.0145	0.2808	0.3800	-0.0333	0.0601	-0.0625
	case 47	(2,2,2,2)	0.2784	0.3904	0.0133	0.2720	0.3843	-0.0527	0.0607	-0.0702

Table 9b Wind-induced lateral-torsional coupled accelerations atop the building with different ratios of torsional to lateral stiffness

	Case No.	Coordinate of mass and rigidity center (m)	RMS response at geometric center			RMS response at corner ($B/2$, $D/2$)		Covariance response between U_N, V_N **and** θ_N		
		(x_M, y_M, x_R, y_R)	$\sigma_{\ddot{U}_N}$	$\sigma_{\ddot{V}_N}$	$\frac{B}{2}\sigma_{\ddot{\theta}_N}$	$\sigma_{\ddot{U}_{N_c}}$	$\sigma_{\ddot{V}_{N_c}}$	$\sigma_{\ddot{U}_N\ddot{V}_N}$	$\sqrt{B}\sigma_{\ddot{U}_N\ddot{\theta}_N}$	$\sqrt{B}\sigma_{\ddot{V}_N\ddot{\theta}_N}$
ratio=1.5	case 0	(0,0,0,0)	0.6725	1.2427	0.1822	0.6967	1.2560	0.0000	0.0000	0.0000
	case 20	(2,2,0,0)	0.8891	1.0614	0.2975	1.0098	1.1645	0.2080	0.3751	-0.3756
	case 41	(0,0,2,2)	1.0568	0.9284	0.2395	0.8663	1.0026	0.1364	-0.4108	0.4111
	case 47	(2,2,2,2)	0.6728	1.2429	0.2115	0.6993	1.2573	-0.3077	0.0918	-0.0932
ratio=2.0	case 0	(0,0,0,0)	0.6725	1.2427	0.1344	0.6858	1.2499	0.0000	0.0000	0.0000
	case 21	(2,2,0,0)	0.8918	1.0841	0.1863	0.9451	1.1279	0.2032	0.2514	-0.2492
	case 41	(0,0,2,2)	0.6779	1.2398	0.1465	0.6413	1.2201	-0.5389	0.2642	-0.2646
	case 47	(2,2,2,2)	0.6726	1.2428	0.1622	0.6886	1.2518	-0.0002	0.0677	-0.0610
ratio=2.5	case 0	(0,0,0,0)	0.6725	1.2427	0.1042	0.6805	1.2470	0.0000	0.0000	0.0000
	case 21	(2,2,0,0)	0.9101	1.0745	0.1397	0.9409	1.1002	0.1711	0.1938	-0.1907
	case 41	(0,0,2,2)	0.8058	1.1612	0.1112	0.7886	1.1493	-0.3504	0.1996	-0.1997
	case 47	(2,2,2,2)	0.6733	1.2423	0.1313	0.6839	1.2485	-0.3040	0.0533	-0.0414

for the power spectra of overturning moments in across-wind and torsional directions (Choi and Kanda 1993), the lateral-torsional responses of the tall building were numerically evaluated. Previous HFFB model test results have shown that there is usually a relatively strong correlation between the generalized modal forces in across-wind and torsional directions (Zhou, *et al.* 2003),

which should be considered in determining the total wind-induced response of a tall building. Hence, the empirical coherence function between the two generalized modal forces, which was proposed by Liang (2004), is used in this study. The effect of nonlinear mode shapes on the wind-induced response was evaluated based on the calculated mode shapes of the building according to the methods developed by Holmes (1987), Katagiri, *et al.* (1992), and Holmes, *et al*. (2003).

The lateral-torsional coupled displacements atop the building were evaluated and presented in Table 10 using the procedure described in Eqs. (15)~(19). Different eccentricity cases either in the mass center or the rigidity center were considered in the computation. It is shown from the results in this table that the eccentricity effects on the wind-induced response are almost the same as those previously discussed for the results presented in Tables 2~8 for the full 3D analytical model. The differences between the results (at the geometric center in along-wind and across-wind directions) from the reduced 3DOFs model and the full 3D analytical model are relatively small. For the reduced 3DOFs model, the calculated RMS torsional responses at the geometry center are somewhat less sensitive to the eccentricities, either in the mass center or the rigidity center, as

Table 10 Wind-induced lateral-torsional coupled displacements atop the building with eccentricities in the mass and/or rigidity center

Case No.	Coordinate of mass and rigidity center (m)	RMS response at geometric center			RMS response at corner ($B/2$, $D/2$)		Covariance response between U_N, V_N **and** θ_N		
	(x_M, y_M, x_R, y_R)	σ_{U_N}	σ_{V_N}	$\frac{B}{2}\sigma_{\theta_N}$	$\sigma_{U_{N_c}}$	$\sigma_{V_{N_c}}$	$\sigma_{U_N V_N}$	$\sqrt{B}\sigma_{U_N\theta_N}$	$\sqrt{B}\sigma_{V_N\theta_N}$
case 0	(0,0,0,0)	0.2477	0.4103	0.1306	0.2800	0.4306	0.0000	0.0000	0.0000
case 1	(1,0,0,0)	0.2446	0.4073	0.1360	0.2799	0.3941	0.0000	0.0000	-0.1703
case 2	(2,0,0,0)	0.2446	0.4070	0.1392	0.2814	0.3897	0.0000	0.0000	-0.1820
case 3	(3,0,0,0)	0.2446	0.4076	0.1412	0.2824	0.3933	0.0000	0.0000	-0.1772
case 10	(0,1,0,0)	0.2389	0.4095	0.1413	0.2297	0.4421	-0.0033	0.1558	0.0884
case 11	(0,2,0,0)	0.2325	0.4095	0.1530	0.2169	0.4563	-0.0027	0.1744	0.1310
case 12	(0,3,0,0)	0.2294	0.4095	0.1585	0.2174	0.4640	-0.0019	0.1745	0.1501
case 19	(1,1,0,0)	0.2537	0.3904	0.1436	0.2685	0.3835	0.0085	0.1135	-0.1611
case 20	(2,2,0,0)	0.2530	0.3881	0.1509	0.2813	0.3798	0.0107	0.0874	-0.1708
case 21	(3,3,0,0)	0.2545	0.3856	0.1546	0.2898	0.3814	0.0105	0.0685	-0.1647
case 28	(0,0,0,1)	0.2378	0.4095	0.1441	0.3128	0.4430	0.0102	-0.1433	0.0880
case 29	(0,0,0,2)	0.2324	0.4095	0.1596	0.3127	0.4582	0.0182	-0.1354	0.1296
case 30	(0,0,0,3)	0.2336	0.4095	0.1692	0.3026	0.4670	0.0234	-0.0916	0.1477
case 34	(0,0,1,0)	0.2446	0.4053	0.1167	0.2710	0.4713	0.0000	0.0000	0.2102
case 35	(0,0,2,0)	0.2446	0.4015	0.1098	0.2681	0.4877	0.0000	0.0000	0.2542
case 36	(0,0,3,0)	0.2446	0.4007	0.1052	0.2662	0.4902	0.0000	0.0000	0.2622
case 40	(0,0,1,1)	0.2275	0.4195	0.1296	0.2828	0.4906	0.0165	-0.1070	0.2188
case 41	(0,0,2,2)	0.2096	0.4343	0.1330	0.2536	0.5188	0.0129	-0.0516	0.2507
case 42	(0,0,3,3)	0.2514	0.3892	0.1357	0.2756	0.4795	0.0277	0.0750	0.2450
case 46	(1,1,1,1)	0.2451	0.4070	0.1206	0.2705	0.4228	0.0010	0.0381	-0.0381
case 47	(2,2,2,2)	0.2467	0.4052	0.1145	0.2671	0.4179	0.0017	0.0512	-0.0512

Table 11 Wind-induced lateral-torsional coupled displacements atop the building with different ratios of torsional to lateral stiffness

	Case No.	Coordinate of mass and rigidity center (m)	RMS response at geometric center			RMS response at corner ($B/2$, $D/2$)		Covariance response between U_N, V_N **and** θ_N		
		(x_M, y_M, x_R, y_R)	σ_{U_N}	σ_{V_N}	$\frac{B}{2}\sigma_{\theta_N}$	$\sigma_{U_{N_c}}$	$\sigma_{V_{N_c}}$	$\sigma_{U_N V_N}$	$\sqrt{B}\sigma_{U_N\theta_N}$	$\sqrt{B}\sigma_{V_N\theta_N}$
ratio=1.5	case 0	(0,0,0,0)	0.2446	0.3954	0.0502	0.2497	0.4442	0.0000	0.0000	0.1961
	case 20	(2,2,0,0)	0.2654	0.3673	0.0537	0.2699	0.4005	-0.0014	0.0220	0.1504
	case 41	(0,0,2,2)	0.2718	0.3814	0.0459	0.3651	0.4295	0.0714	0.0838	0.1921
	case 47	(2,2,2,2)	0.2454	0.3925	0.0432	0.2325	0.4233	-0.0004	0.0897	0.1524
ratio=2.0	case 0	(0,0,0,0)	0.2446	0.3954	0.0272	0.2461	0.4226	0.0000	0.0000	0.1467
	case 21	(2,2,0,0)	0.2624	0.3722	0.0283	0.2633	0.3934	-0.0020	0.0177	0.1242
	case 41	(0,0,2,2)	0.2372	0.4091	0.0238	0.2443	0.4322	-0.1253	0.0632	0.1374
	case 47	(2,2,2,2)	0.2450	0.3938	0.0232	0.2370	0.4107	-0.0002	0.0665	0.1145
ratio=2.5	case 0	(0,0,0,0)	0.2446	0.3954	0.0172	0.2452	0.4128	0.0000	0.0000	0.1173
	case 21	(2,2,0,0)	0.2386	0.4025	0.0178	0.2388	0.4155	-0.0135	0.0147	0.1017
	case 41	(0,0,2,2)	0.2788	0.3694	0.0197	0.2588	0.3854	0.0002	0.0505	0.1082
	case 47	(2,2,2,2)	0.2449	0.3943	0.0146	0.2395	0.4051	-0.0001	0.0529	0.0916

compared to those from the 3D analytical model. Some differences in the covariance responses and RMS responses at the upper-right corner exist between the calculated results from these two different approaches. The major reason for these differences may be attributed to adoption of the different empirical formulas for the power spectra of the aerodynamic forces in the dynamic analysis.

The wind-induced lateral-torsional responses of the tall building calculated from the reduced 3DOFs model are shown in Table 11, in which the torsional stiffness values were assumed to be the same as those for the cases considered in Table 9. The eccentricity effects on the wind-induced responses presented in Table 11 are about the same as those previously discussed for Table 9. As shown in Table 11, the RMS torsional responses and the covariance responses between the along-wind and torsional responses at the geometry center dramatically reduced when the eccentricity either in the mass or the rigidity center was presented. But, the covariance responses between the across-wind and torsional directions, calculated from the reduced 3DOFs model, were much less affected by the torsional stiffness and the eccentricities. Since the statistical coupling between the generalized across-wind forces and torsional moments was considered in the dynamic analysis of the reduced 3DOFs model, such coupling contributed to the covariance responses between the across-wind and torsional directions significantly, as compared to the case of the mechanical coupling effect. This may be a possible reason for the less variation of the covariance responses as discussed previously.

5. Conclusions

Based on the empirical formulas for the power spectra of overturning moments and local fluctuating across-wind forces and torsional moments, the wind-induced lateral-torsional coupled response analysis of a rectangular tall building was performed in this study. By setting various parameters such as the

eccentricities in the mass and/or the rigidity center and considering different ratios of the torsional to lateral stiffness, the eccentricity effects on the lateral-torsional motions of a rectangular tall building were studied comprehensively through the full 3D analytical model and reduced 3DOFs model. Some conclusions were summarized as follows:

(1) To examine the accuracy and effectiveness of the adopted empirical formulas and the computational procedure presented in this paper, the along-wind, across-wind and torsional responses of the tall building without eccentricity were calculated and compared with the available wind tunnel test results. The satisfactory agreement between the calculated results and the experimental data demonstrated the applicability of the methods presented in this paper.

(2) The eccentricities in the mass or the rigidity center may significantly affect the torsional responses at the geometric center of the building. In some cases, the covariance responses between the along-wind (or across-wind) and torsional directions were found to be in the same order of magnitude as the along-wind or across-wind responses, suggesting that the lateral-torsional coupled effect on the overall wind-induced response can not be neglected for such cases.

(3) The torsional motion contributed significantly to the overall lateral-torsional coupled responses of the tall building with eccentricities in the mass and/or the rigidity center. Through extensive numerical studies, it was found that the effects of eccentricities in the mass and/or the rigidity center as well as the torsional stiffness on the lateral-torsional acceleration responses are more significant than those on the displacement responses.

(4) The lateral-torsional responses calculated by the reduced 3DOFs model were in good agreement with those obtained by the full 3D analytical model, even though different empirical formulas for the power spectra of the wind loads were adopted for these two cases. Therefore, it was concluded that the wind-induced lateral-torsional responses of rectangular tall buildings can be effectively determined by utilizing the selected empirical formulas for the aerodynamics wind loads which were derived from extensive HFFB and SMPSS wind tunnel tests.

(5) The framework presented in this paper provides a useful tool to evaluate the wind-induced lateral-torsional coupled responses of rectangular buildings, which will enable structural engineers in the preliminary design stages to assess the serviceability of tall buildings, potential structural vibration problems and the need for a detailed wind tunnel test.

Acknowledgment

The work described in this paper was fully supported by a research grant from the Research Committee of City University of Hong Kong (Project No. 7002104). The financial support is gratefully acknowledged.

References

Architectural Institute of Japan (1996), *AIJ Recommendations for Loads on Buildings.*

Cao, H. and Li, Q. S. (2004), "New control strategies for active tuned mass damper systems", *Comput. Struct.*, **82**, 2341-2350.

Cermak, J.E. (2003), "Wind-tunnel development and trends in applications to civil engineering", *J. Wind Eng.*

Ind. Aerodyn., **91**, 355-370.
Chen. X.Z. and Kareem, A. (2005), "Coupled dynamic analysis and equivalent static wind loads on buildings with three-dimensional modes", *J. Struct. Eng., ASCE*, **131**(7), 1071-1082
Choi, H. and Kanda, J. (1992), "Correlating dynamic wind force components on 3-D cylinders", *J. Wind Eng. Ind. Aerodyn.*, **41-44**, pp.785-796
Choi, H. and Kanda, J. (1993), "Proposed formulae for the power spectral densities of fluctuating lift and torque on rectangular 3-D cylinders", *J. Wind Eng. Ind. Aerodyn.*, **46-47**, 507-C516.
Davenport, A.G. (1967), "Gust loading factors", *J. Struct. Div., ASCE,* **93**(ST3), 23-28.
Holmes, J.D. (1987), "Mode shape corrections for dynamic response to wind", *Eng. Struct.*, **l9**, 210-212.
Holmes, J.D. (2001), *Wind Loading of Structures,* Spon Press, London.
Holmes, J., Rofail, A. and Aurelius, L. (2003), "High frequency base balance methodologies for tall buildings with torsional and coupled resonant modes", *The 11th International Conference on Wind Engineering,* USA.
Islam, M.S. (1988), "Modal coupling and wind-induced vibration of tall buildings", Ph.D. Thesis, The Johns Hopkins University, Baltimore, Maryland, USA.
Islam, M.S. and Ellingwood, B. (1992), "Wind-induced response of structurally asymmetric high-rise buildings", *J. Struct. Eng.*, **118**(1), 207-222.
Isyumov, N. (1982), "The aeroelastic modelling of tall buildings", *Wind Tunnel Modelling for Civil Engineering Applications*, Cambridge University Press.
Li, Q.S., Fang, J.Q., Jeary, A.P. and Wong, C.K. (1998), "Full scale measurements of wind effects on tall buildings", *J. Wind Eng. Ind. Aerodyn.*, **74-76**, 741-750.
Li, Q.S. (2000), "Evaluation of wind-induced vibration of tall buildings and reliability analysis: a case study", *Hong Kong Institution of Engineers, Transactions*, **7**(1), 47-50.
Li, Q.S., Liu, D.K., Fang, J.Q. and Tam, C.M. (2000), "Multilevel optimal design of tall buildings with active control under winds using genetic algorithms", *J. Wind Eng. Ind. Aerodyn.*, **86**(1), 65-86.
Li, Q.S., Yang, K, Wong, C.K. and Jeary, A.P. (2003), "The effect of amplitude-dependent damping on wind-induced vibrations of a super tall building", *J. Wind Eng. Ind. Aerodyn.*, **91**, 1175-1198.
Li, Q.S., Wu, J.R., Liang, S.G., Xiao, Y.Q. and Wong, C.K. (2004), "Full scale measurements and numerical evaluation of wind-induced vibration of a 63-storey reinforced concrete tall building", *Eng. Struct.*, **26**, 1779-1794.
Li, Q.S., Xiao, Y.Q. and Wong, C.K. (2005), "Full-scale monitoring of typhoon effects on super tall buildings", *J. Fluids Struct.*, **20**, 697-717.
Liang, B., Tamura, Y. and Suganuma, S. (1997), "Simulation of wind-induced lateral-torsional motion of tall buildings", *Comput. Struct.*, **63**(3), 601-606.
Liang, B. (2004), Mathematical model of the aerodynamic forces, http://www.wind.arch.t-kougei.ac.jp/info_center/other.html.
Liang, S.G., Liu, S.C., Li, Q.S., Zhang, L.L. and Gu, M. (2002), "Mathematical model of acrosswind dynamic loads on rectangular tall buildings", *J. Wind Eng. Ind. Aerodyn.*, **90**(12-15), 1757-1770.
Liang, S.G., Li, Q.S., Zou, L.H. and Wu, J.R. (2005), "Simplified formulas for evaluation of across-wind dynamic responses of rectangular tall buildings", *Wind Struct.*, **8**(3), 197-212.
Kan, C.L. and Chopra, A.K. (1977), "Elastic earthquake analysis of torsionally coupled multistory buildings", *Earthquake Eng. Struct. Dyn.*, **5**, 395-412.
Kareem, A. (1992a), "Lateral-torsional motion of tall buildings to wind loads", *J. Struct. Eng., ASCE*, **111**(11), 2479-2496.
Kareem, A. (1992b), "Dynamic response of high-rise buildings to stochastic wind loads", *J. Wind Eng. Ind. Aerodyn.,* **41-44**, 1101-1112.
Katagiri, J., Nakamura, O., Ohkuma, T., Marukawa, H., Tsujimoto, T. and Kondo, K. (1992), "Wind-induced lateral-torsional motion of tall building", *J. Wind Eng. Ind. Aerodyn.,* **41-44**, 1127-1137.
Lin, N., Letchford, C., Tamura, Y., Liang, B. and Nakamura, O. (2005), "Characteristics of wind forces acting on tall buildings", *J. Wind Eng. Ind. Aerodyn.*, **93**(3), 217-242.
Safak, E. and Foutch, D.A. (1987), "Coupled vibrations of rectangular buildings subjected to normally-incident random loads", *J. Wind Eng. Ind. Aerodyn.*, **126**, 129-148.
Simiu, E. and Scanlan, R.H. (1996), *Wind Effects on Structures: Fundamentals and Applications to Design*. John Wiley & Sons, Inc.

Tallin, A. (1984), "Wind induced motion of tall buildings", Ph.D. Thesis, The Johns Hopkins University, Baltimore, Maryland, USA.
Tallin, A. and Ellingwood, B. (1985), "Wind-induced lateral-torsional motion of buildings", *J. Struct. Eng.*, **11**(10), 2197-2213.
Tschanz, T. and Davenport, A.G. (1983), "The base balance technique for the determination of dynamic wind loads", *J. Wind Eng. Ind. Aerodyn.*, **13**(1-3), 429-439.
Tsukagoshi, H., Tamura, Y., Sasaki, A. and Kanai, H. (1993), "Response analyses on along-wind and across-wind vibrations of tall buildings in time domain", *J. Wind Eng. Ind. Aerodyn.,* **46-47**, 497-506.
Vickery, P.J., Steckley, A., Isyumov, N. and Vickey, B.J. (1985), "The effect of mode shape on the wind-induced response of tall building", *The 5th U. S. National Conference on Wind Engineering*, pp. 1B41-1B48.
Wu, J.R., Liu, P.F. and Li, Q.S. (2007), "Effects of nonlinear damping and time constant on wind-induced responses of a 79-storey tall building", *Comput. Struct.*, **85**, 1014-1021.
Xu, Y.L. and Kwok, K.C.S. (1987), "Mode shape corrections for wind tunnel tests of tall buildings", *Eng. Struct.*, **15**(5), 387-392.
Yoshida, M., Kondo, K. and Suzuki, M. (1992), "Fluctuating wind pressure measured with tubing system", *J. Wind Eng. Ind. Aerodyn.*, **42**, 987-998.
Zhou, Y., Kijewski, T. and Kareem, A. (2003), "Aerodynamic loads on tall buildings: interactive database", *J. Struct. Eng.*, **129**(3), 394-404.

CC